The Gamma Rays of the Decay of Uranium-233 Populating States in Thorium-229

A Thesis

Submitted to

the

Faculty of Graduate Studies

In Partial Fulfilment

of the Requirement for the Degree

MASTER OF SCIENCE

---

by

Beverley Pople

June 1975

THE GAMMA RAYS OF THE DECAY OF URANIUM-233 POPULATING STATES IN THORIUM-229

by

Beverley Pople

A dissertation submitted to the Faculty of Graduate Studies of the University of Manitoba in partial fulfillment of the requirements of the degree of

MASTER OF SCIENCE

ACKNOWLEDGEMENTS

I would like to express my sincere appreciation to Dr. M. Canty of the Physics Department, University of Manitoba for his enlightening discussions and his assistance in the coincidence work and to Dr. D. Dohan also of the Physics Department for the development of computer programs required for the analysis of the coincidence data. Also gratefully acknowledged is Mr. D. Buksak of the Chemistry Department of the University of Manitoba for preparation of the active materials. My greatest thanks go to my advisor, Dr. R. D. Connor, for his patience and understanding and for never being too busy to help me. Finally, I wish to thank my parents for all that they have done for me and my fiancé, Doug Emek, for his constant love and encouragement.

TO MY PARENTS

ABSTRACT

The decay of U-233 was examined using Ge(Li) and Si(Li) gamma ray spectrometers. Chemical separation of the contaminating daughter products were effected through anion exchange. One hundred and fourteen gamma rays were identified in the singles spectrum of which eighteen are reported here for the first time: 31.52, 68.87, 72.88, 74.86, 77.13, 85.43, 86.77, 87.27, 88.46, 116.41, 176.13, 177.81, 185.81, 226.72, 252.53, 260.65, 295.17, and 351.81 keV. Gamma-gamma coincidence measurements were used to study the level diagram of the excited states of Th-229. For the first time in this laboratory a computer was incorporated into the coincidence system which allowed for the simultaneous collection of all coincidence events. This new method was used as opposed to the time consuming single gating method. Several new gamma rays were proposed as linking transitions: 14.44, 27.33, 76.98 and 138.5 New levels were proposed at 235,340 and 478.74 keV.

Table of Contents

Figures

Figures

Tables

CHAPTER I

INTRODUCTION

Three radioactive series are naturally occurring in nature, viz., the (4n+2) Uranium-Radium series, the (4n+3) Actinium series and the (4n) Thorium series. The (4n+1) series is absent in nature, but it has been produced artificially. This series is known as the Neptunium series, named after its longest living member, ^{237}Np. Previous work in this laboratory has included detailed studies of the Actinium series.[1] The present work endeavours to investigate the decay of a long lived member of the Neptunium series, namely ^{233}U.

Since the Neptunium series does not occur naturally, its constituent elements would not be as well known as they are today, had it not been for the discovery of artificial radioactivity. Due to the importance of this phenomenon with respect to the Neptunium series, a brief discussion will be given.

Roentgen's discovery of X-rays in 1895 was followed one year later by the discovery of radioactivity by Henri Becquerel. In the years that followed, many important discoveries of naturally occurring radioactive elements were made. However, in 1919, Rutherford made a discovery that indicated the existence of a new field of research. While testing the range of alpha particles from radium in

nitrogen, he observed that the alpha rays gave rise to a different type of radiation, which caused a fluorescent screen to scintillate. What Rutherford was actually observing was the transformation of nitrogen atoms by alpha particles into radioactive fluorine atoms which then decayed into the protons that were detected on the screen according to the reaction,

$$^{14}_{7}N + ^{4}_{2}He \longrightarrow [^{18}_{9}F] \longrightarrow ^{17}_{8}O + ^{1}_{1}H$$

This discovery indicated the possible breakdown of an atomic nucleus by a rapidly moving particle.

In 1934, Curie and Joliot observed for the first time the production of artificial radioactivity. By bombarding boron and aluminum with alpha particles, they produced radioactive nitrogen and phosphorous.

$$^{10}_{5}B + ^{4}_{2}He \longrightarrow ^{13}_{7}N + ^{1}_{0}n \qquad ^{13}_{7}N \xrightarrow{\beta^+} ^{13}_{C}$$

$$^{27}_{13}Al + ^{4}_{2}He \longrightarrow ^{30}_{15}P + ^{1}_{0}n \qquad ^{30}_{15}P \xrightarrow{\beta^+} ^{30}_{Si}$$

Before the idea of artifical radioactivity could be applied to heavy elements, new techniques had to be developed to produce bombarding particles of sufficiently high energy to penetrate the Coulomb barrier of the heavy elements. However, with the development and widespread use of particle accelerators this goal was reached and since that time many radioactive nuclides have been identified.

The Neptunium series is named after its longest living member and not after the parent nucleus. The first eight elements of the series are artificially produced

transuranic elements namely, californium-253, einsteinium-253, berkelium-249, californium-249, curium-245, plutonium-241, americium-241 and neptunium-237. The subsequent members are isotopes of elements that do occur in nature, viz., protactinium-233, uranium-233 and so on, ending with bismuth-209 which is stable. All of the transuranic elements have been discovered since 1940 with the parent element, californium, being identified in 1950 by Thompson, Street, Ghiorso and Seaborg.[2] This was produced by bombarding another artificially produced element, curium, with high energy alpha particles.

Uranium-233 is an important member of the Neptunium series because it serves as a suitable source for the study of its shorter lived descendants. Uranium-233 can be produced artificially by neutron capture in thorium in a nuclear reactor according to the reaction:

$$^{232}Th(n,\gamma)^{233}Th;\ ^{233}Th \xrightarrow[23\ min]{\beta^-} {}^{233}Pa \xrightarrow[27.4\ day]{\beta^-} {}^{233}U$$

Relative large amounts of ^{233}U are required for nuclear spectroscopy because 83% of all decays proceed to the ground state. Only 17% populates the excited states, the de-excitation of which produces the gamma rays observed. Further, the half life of ^{233}U is greater than 10^5 years, so it is necessary to have at least milligram amounts of ^{233}U in order to study its decay products.

Uranium-233 was first separated and examined in 1941-1942 by Seaborg, Gofman and Stoughton.[3] It was produced by

irradiating thorium with cyclotron produced neutrons. They observed that it decayed by emitting alphas and they made a rough determination of its half life, which they found to be 1.2×10^6 years. Since its discovery, many measurements of the half life of ^{233}U have been made and the accepted value is now 1.62×10^5 years.[4] The conversion electron spectra, alpha decay and gamma decay of ^{233}U have all been studied in a preliminary way and the earlier references are documented in literature.[5] The most recent work on the gamma decay has been done by Ahmad[6] (1966), Cline[7] (1971) and Kroger[8] (1972).

CHAPTER II

EQUIPMENT AND METHODS

I. INTRODUCTION

The introduction of semiconductor detectors into the field of nuclear spectroscopy was an extremely important development. The advantage of these detectors over conventional scintillation detectors is their ability to resolve photopeaks which lie very close in energy. Although scintillation detectors have superior efficiencies compared to semiconductor detectors, the efficiency of a semiconductor detector can be improved by increasing the sensitive volume of the detector. In spite of this disadvantage, semiconductor detectors are invaluable for accurate energy determinations because of their superior resolution.

Two types of semiconductor detectors have been used in the present work. They are lithium drifted germanium Ge(Li) and lithium drifted silicon Si(Li) detectors. Si(Li) detectors are useful for studying X-rays and gamma rays whose energies are below 40 keV. In the region of 35 keV, Ge(Li) detectors have approximately ten times the background of corresponding Si(Li) devices.[9] The reason for this is that in this energy region the Si(Li) detectors are much less sensitive to background gamma radiation owing to silicon's low cross section for photoelectric absorption and in particular to low cross sections for the Compton

interactions from higher energy radiation. Above 40 keV, the efficiency of Si(Li) detectors decreases so rapidly the Ge(Li) detectors are essential. A list of the detectors used in this study and their specifications is given in Table I.

TABLE I

DETECTORS

DETECTOR	SIZE	RESOLUTION	WINDOW	OPERATING VOLTAGE
NUCLEAR DIODE Ge(Li)	50 cc	2.05 keV at 1.33 MeV	0.5 mm Al	+3000 volts
ORTEC Ge(Li) X-ray #1	80 mm^2	230 eV at 6.5 keV	0.13 mm Be	-800 volts
		600 eV at 122 keV		
ORTEC Ge(Li) X-ray #2	50 mm^2	625 eV at 122 keV	0.13 mm Be	-900 volts
KEVEX Si(Li) X-ray	80 mm^2	218 ev at 5.96 keV	0.03 mm Be	+1000 volts
ORTEC Ge(Li)	52 cc	1.95 keV at 1.33 MeV	0.5 mm Al	+4800 volts
NUCLEAR DIODE Ge(Li)	30 cc	2.14 keV at 1.33 MeV	0.5 mm Al	+2500 volts

II. SINGLES

A. EQUIPMENT

When studying a particular radiosotope, the initial step is to use a Ge(Li) detector to obtain a gamma ray spectrum. This is referred to as a singles measurement and the experimental arrangement is shown in Figure 1. Once a gamma ray emitted by the source reaches the detector crystal and deposits its energy, a signal whose pulse height is proportional to the energy of the incoming gamma ray is sent through the preamplifier. This preamp pulse is then fed into an amplifier where it is further amplified before being sent to the analysis and storage unit of the multi-channel analyzer (MCA). The MCA contains analogue to digital converters (ADC's) where the pulse heights of the various incoming pulses are stored in particular channels, with each channel corresponding to a different pulse height and hence energy.

Throughout this work, Canberra 1417B spectroscopy amplifiers and Ortec Model 472 amplifiers were used and the multi-channel analyzer was a Nuclear Data Model ND-2200 (Nuclear Data, Inc., Palantine, Illinois). This particular analyzer had three ADC's with a total memory capacity of 4096 channels which can be divided between the three ADC's in such a way that all three units could be operated independently at the same time.

B. DATA ANALYSIS

Once the data is stored in the multi-channel analyzer, the output can be presented in one of two ways. A

FIGURE 1

SINGLES MEASUREMENTS

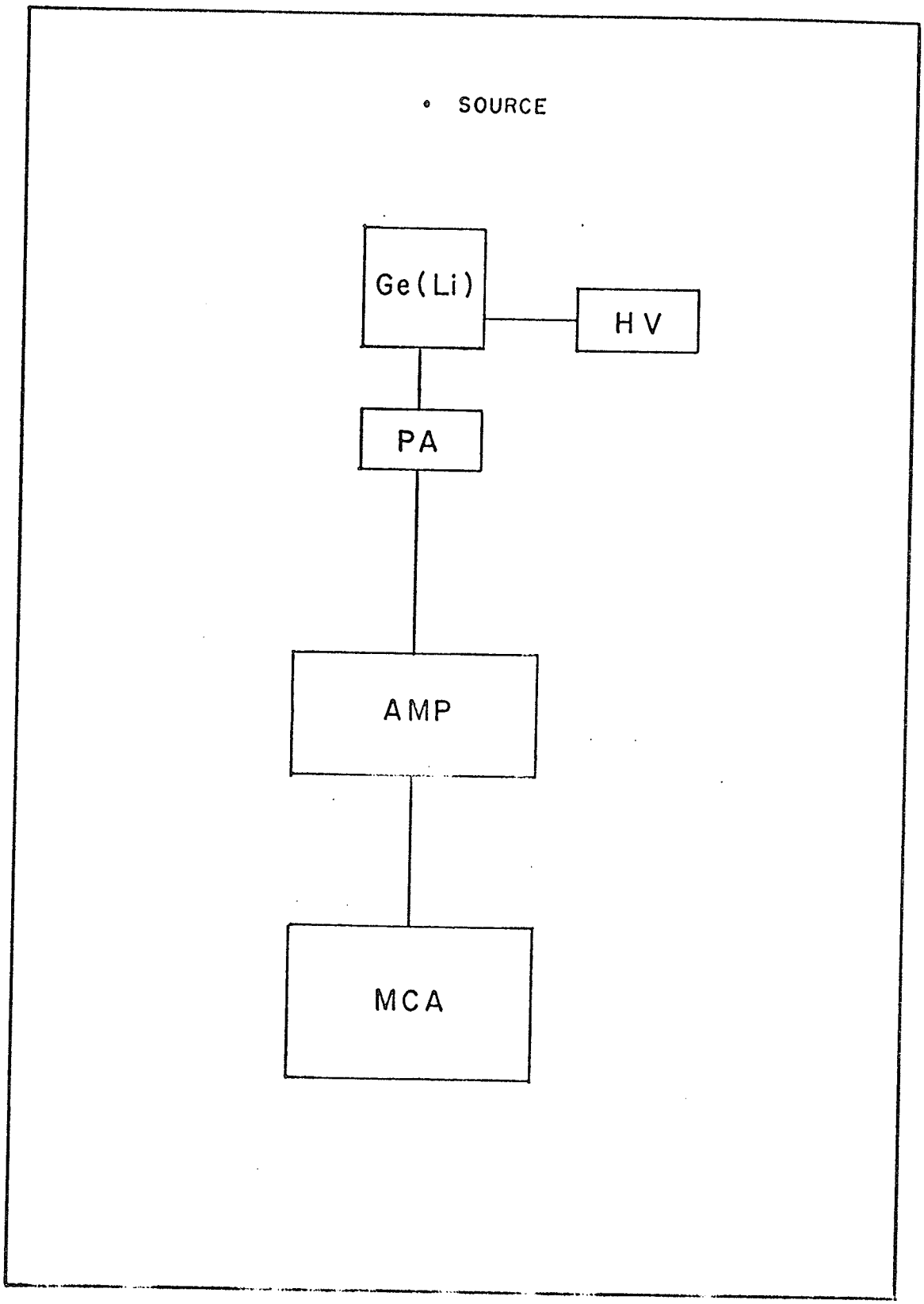
SOURCE
Ge(Li)
HV
PA
AMP
MCA

two dimensional x-y plot may be obtained which can be studied immediately or the data can be punched on paper tape to await its later conversion into cards for computer processing. The procedure is that the paper tape output is fed into a teletype terminal located in the laboratory which is coupled to an IBM-370 computer. The data can then be stored directly on magnetic disk in the computer, or converted to cards first and then put on magnetic disk.

Once the data are stored in the computer, analysis programs can be run directly from the terminal in the laboratory. Several computer programs have been developed in this laboratory to perform the analysis. CUTIPIE[10] is a program that accurately determines the position and areas of photopeaks giving the energy and intensity of the radiations. The program consists of two main parts. Initially, an automatic peak searching process occurs followed by the fitting of an analytical function to the photopeak. The simplest shape is used for peaks that have poor statistics and it is a pure gaussian distribution fitted onto a straight line background. A more sophisticated peak shape, which is most commonly used, consists of a gaussian distribution with an exponential tail on the low energy side, fitted onto a background function that resembles a Fermi distribution.

In order to initiate the automatic peak searching process, the only input information required is the data and the approximate value of the full width of the photopeak at

half maximum (FWHM). A manual peak-searching process is also a feature of the program in which the programmer gives as input data the approximate positions of the peaks to be fitted and the region in which the peaks lie. The program was written in such a way that up to six overlapping peaks can be unfolded. This restriction to six is due to the assumption that the lines in a region of overlapping photo-peaks all have the same width. To go to more than six peaks with a single FWHM invites errors as the width increases with energy.

III. GAMMA-GAMMA COINCIDENCE MEASUREMENTS

A. EQUIPMENT

Once the energies and intensities of the radiations from any isotope are known, information on the time correlations between the gamma rays must be obtained before a decay scheme can be proposed. This information is obtained from gamma-gamma coincidence measurements, which allow for the observation of cascading gamma rays, as the various excited states de-excite to the ground state.

Two Ge(Li) detectors of volumes 30 cc. and 52 cc. positioned at an angle of 180^{o} were used for the coincidence measurements in the present work. The ^{233}U source was deposited and evaporated to dryness in a recess 1/16" in depth and 1/4" in diameter which was milled in a plexiglas plate and the source was covered with a 1/16" plexiglas disk. This plate was then sealed between two lead plates, each of dimensions 5"x5" and 1/8" thick which had holes concentric with the location of the source. The lead plates containing the source were placed between the two detectors which were then positioned so that each detector face was as close to the lead plates as possible. This particular choice of geometry with the source visible but surrounded by lead was made in order to reduce the possibility of back-scattering from one detector into the other which would lead to spurious coincidences.

The conventional method of gamma-gamma coincidence measurements was not used in the present work; rather than

using the time consuming method of selecting a single gamma ray as a "gate" and observing the gamma rays in coincidence with it, a computer was incorporated into the system to allow for the simultaneous collection of all gamma rays in coincidence. In this way, information on all the gamma rays in coincidence with one another was obtained in a single experiment in a few days and during the analysis process, gating lines were then chosen and the data was sorted to give the coincidence spectrum for each gating line. Using the single gating method, the gating lines are chosen first and for each one the experiment must be run separately, which for any large number of gating lines requires several weeks and can run into months.

The coincidence circuitry is shown in Figure 2. The output pulse from each detector is divided into two parts (a) and (b).

(a) The detector timing output (T) furnishes output pulses for timing measurements. In order to compensate for the different risetimes of pulses of varying pulse heights, the amplitude risetime compensation method of deriving pulses from the detectors was used. This involved the use of an Ortec Model 454 timing filter amplifier (TFA) and an Ortec Model 463 constant fraction discriminator (CFTD). The 454 amplifies the output of the preamplifier to a large enough amplitude to fire the 463. During the amplification process, the fast rise time of the preamplifier pulses is

FIGURE 2

GAMMA-GAMMA COINCIDENCE SYSTEM

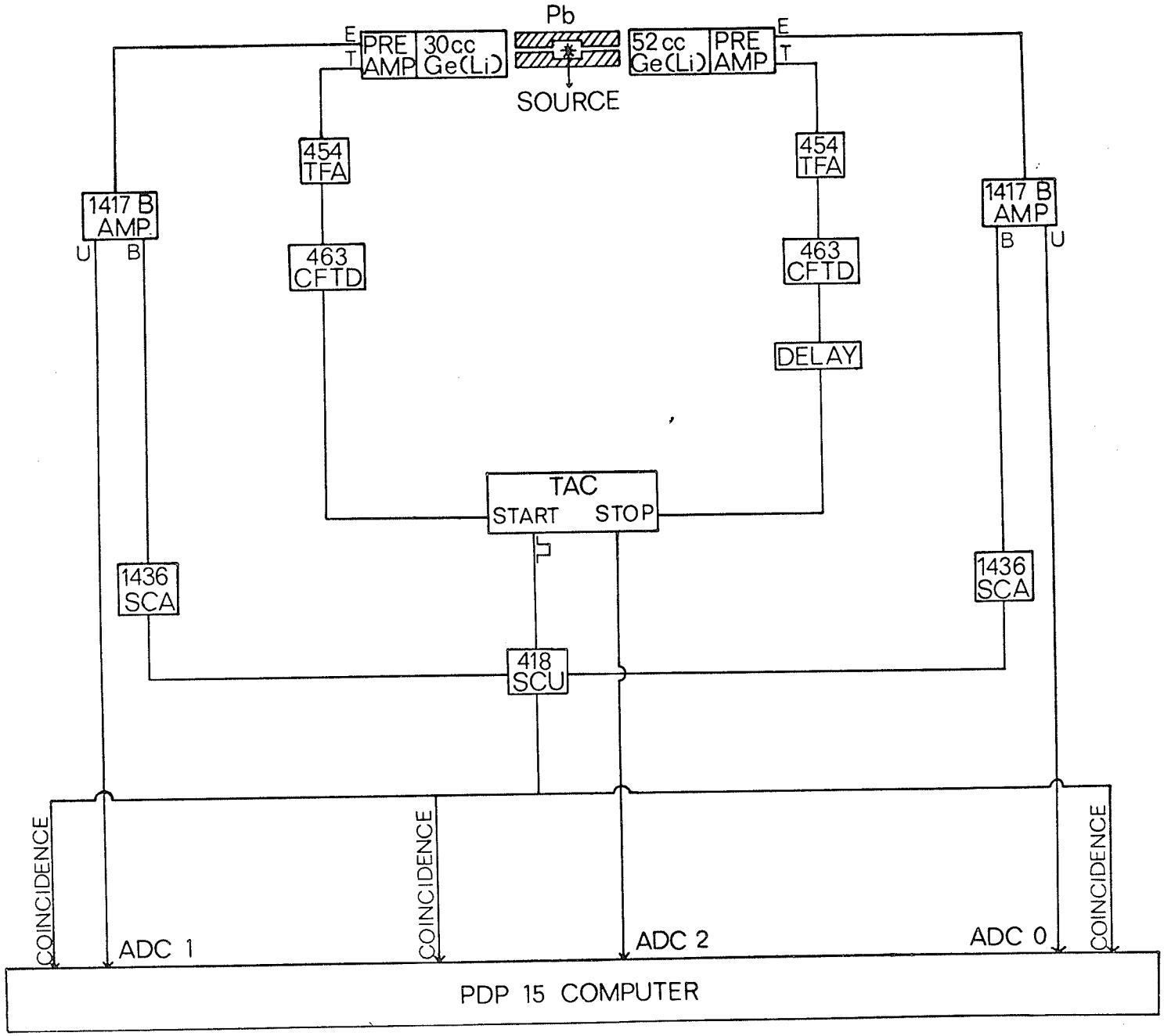
Pb
E
T
PRE AMP
30cc Ge(Li)
SOURCE
52 cc Ge(Li)
PRE AMP
E
T
454 TFA
454 TFA
1417 B AMP
U
B
463 CFTD
463 CFTD
1417 B AMP
B
U
DELAY
TAC
START
STOP
1436 SCA
1436 SCA
418 SCU
COINCIDENCE
ADC 1
COINCIDENCE
ADC 2
ADC 0
COINCIDENCE
PDP 15 COMPUTER

also retained. The 463 eliminates timing walk which is caused by energy and pulse shape variations. Rather than detecting pulses at a preset discriminator level which would result in a time difference between pulses of various heights, the 463 detects pulses at a certain constant fraction of their individual pulse heights. When the 463 detects the leading edge of a pulse, i.e. when it experiences a sharp increase in voltage, a logic pulse is generated.

The pulse originating in the 52 cc. detector is now delayed by 7.5 nsec. while the pulse coming from the 30 cc. detector is fed directly into the start input of a Conuclear Ltd. C126 time to analogue converter (TAC). The delayed time pulse from the 52 cc. detector is used for the stop input of the TAC. The timing output of the TAC produces pulses whose heights are proportional to the time interval between the start and stop pulses. In order for two pulses to start and stop the TAC, they must arrive within the selectable range of the TAC, which was chosen to be 200 nanoseconds. This output is fed directly into ADC2. A second TAC output produces logic pulses which are generated each time a coincident event occurs, i.e. each time two pulses arrive within the range of 200 nanoseconds. These logic pulses provide input pulses for the Ortec Model 418 universal coincidence unit.

(b) The energy outputs (E) of both detectors are amplified in Canberra Model 1417 spectroscopy amplifiers. The prompt

bipolar pulses (B) from each of the two amplifiers are fed into Canberra Model 1436 timing single channel analyzers (SCA) whose discriminator levels are set just above the noise level. The two logic pulses from the individual SCA's serve as the energy input pulses for the 418 slow coincidence unit (SCU).

The delayed unipolar pulses (U) from each amplifier go directly into the remaining two ADC's.

Thus, two ADC's are fed pulses proportional to the energies of the gamma rays being detected in the two Ge(Li) detectors while the third ADC receives a pulse whose height is proportional to the time interval between the detection of the two gamma rays.

The three ADC's are interfaced to a Digital Equipment Corporation PDP-15 computer. As mentioned earlier, the incorporation of the computer into the system allows for the simultaneous collection of all gamma rays in coincidence as opposed to the time consuming single gate conventional method. Each time the three gates of the slow coincidence unit are opened, indicating that the time and energy requirements have been met, the three analogue pulses are routed by the ADC's into addresses defined by E1, E2, and T. Once the process is complete this information is stored in a buffer of 512 words. When the buffer is full, all of the information is transferred onto magnetic tape.

B. DATA ANALYSIS

Once all of the data is stored on magnetic tape, they

are sorted into its three projections viz., an E1 projection which is the coincidence spectrum from the 52 cc. detector, an E2 projection which is the coincidence spectrum from the 30 cc. detector and a TAC projection which is the time spectrum of the TAC. The 52 cc. detector was used as the gating detector and windows were set using the E1 projection. A maximum total of 12 gates could be set at any one time, in addition to the gate setting the discriminator levels for the output time pulse of the TAC. In the present work only 10 gates were selected and for each gate 10 individual coincidence spectra were obtained each consisting of 1024 channels. These correspond exactly to 10 SCA spectra taken in the traditional way. Corresponding to each gate that was set on a particular photopeak, a gate was also chosen for a suitable background region and the background coincident spectra were obtained. For any gating line, background contributes to the coincidence spectrum, so the background coincidence spectrum must be subtracted from the composite spectrum to give the residual coincidence spectrum. Random coincidences were neglected throughout this work and this is explained later in Chapter IV.

CHAPTER III

CALIBRATION

I. ENERGY CALIBRATION

Before any accurate information can be obtained from a spectrum taken with any semiconductor detector, the particular detector system must be calibrated so that it is possible to determine the energies and intensities of the photopeaks.

The technique used for energy calibration was the mixed source approach. This involves obtaining the spectra of the isotope under study simultaneously with the spectra of one or more calibration sources whose energies are very well known (see Table II).[11,12] In addition to the gamma ray standards, characteristic X-rays were also used as calibration lines[13] (see Table III). Siegbahn notation is used.[14]

Once the composite spectrum of the mixed sources is obtained, two calibration lines which are suitably placed, so that the uncalibrated lines from the source under examination fall in the region between them, are chosen as fixed calibration points. To a first approximation, a linear relationship is assumed between energy and channel number, namely:

$$E=MX+B$$

where E is the photopeak energy, X is the channel number, M is the conversion gain (keV/channel) and B is the energy

TABLE II

CALIBRATION ENERGIES

Calibration Source	Half Life	Energy (keV)
Am-241	432.9 years	11.9 ± 0.1
		13.9 ± 0.1
		26.345 ± 0.001
		59.537 ± 0.001
Ba-133	10.5 years	80.997 ± 0.005
		276.397 ± 0.012
		302.851 ± 0.015
		356.005 ± 0.017
		383.851 ± 0.020
Co-57	271.6 days	122.061 ± 0.010
		136.471 ± 0.010
Co-60	5.3 years	1173.23 ± 0.04
		1332.49 ± 0.05
Cs-137	30.6 years	661.635 ± 0.076
Mn-54	312.6 days	834.81 ± 0.03
Na-22	2.6 years	511.006 ± 0.002
Ta-182	115 days	67.750 ± 0.001
		84.680 ± 0.002
		100.105 ± 0.001
		152.434 ± 0.002
		156.387 ± 0.002
		179.393 ± 0.003
		198.356 ± 0.004
		222.110 ± 0.003
		229.322 ± 0.006
		264.072 ± 0.006

TABLE III

X-RAY CALIBRATION ENERGIES

X-ray	Energy (keV)
Ag $K_{\alpha 2}$	21.9903±0.0002
Ag $K_{\alpha 1}$	22.1629±0.0002
Ag $K_{\beta 1}$	24.9424±0.0002
Ag $K_{\beta 2}$	25.4564±0.0002
Ba $K_{\alpha 2}$	31.8171±0.0004
Ba $K_{\alpha 1}$	32.1936±0.0003
La $K_{\alpha 2}$	33.0341±0.0002
La $K_{\alpha 1}$	33.4418±0.0002
La $K_{\beta 1}$	37.8010±0.0003
La $K_{\beta 2}$	38.7299±0.0008
Yb $K_{\alpha 2}$	51.3540±0.0004
Yb $K_{\alpha 1}$	52.3889±0.0004
W $K_{\alpha 2}$	57.983 ±0.001
W $K_{\alpha 1}$	59.320 ±0.001
Bi $K_{\alpha 2}$	74.8148±0.0009
Bi $K_{\alpha 1}$	77.1079±0.0010
Th $K_{\alpha 2}$	89.953 ±0.001
Th $K_{\alpha 1}$	93.350 ±0.001

intercept which corresponds to the digital zero shift on the ADC. From the two calibration energies and their positions, values of the parameters M and B are determined.

Once the parameters are determined, it is not possible to determine the energies of other photopeaks in the spectra by merely substituting their positions into the formula E=MX+B. This would be valid if the system were truly linear, but the amplifiers and ADC's produce a non-linearity which necessitates adding a correction term δ to the energy. The quantity δ measures the deviation of the system from linearity and it is the difference between the known energy of a photopeak and its energy calculated from E=MX+B. Hence the correct equation for the actual photopeak energy is:

$$E = E_{calculated} + \delta$$
$$= MX + B + \delta$$

The calibration run involving the mixed sources is used to determine the non-linearity curve of the system which is a plot of δ vs channel number using the known peaks. The positions of all the calibration peaks are substituted into $E=MX+B+\delta$ to determine the values of δ. The two calibration peaks which were used to determine the parameters M and B will have a $\delta=0$ deviation from linearity while all other deviations will be non-zero. Using the value of δ obtained in this manner the non-linearity curve is drawn. An example of such a curve is shown in Figure 3. The calibration sources used were tantalum-182 and barium-133.

FIGURE 3

NON-LINEARITY CURVE

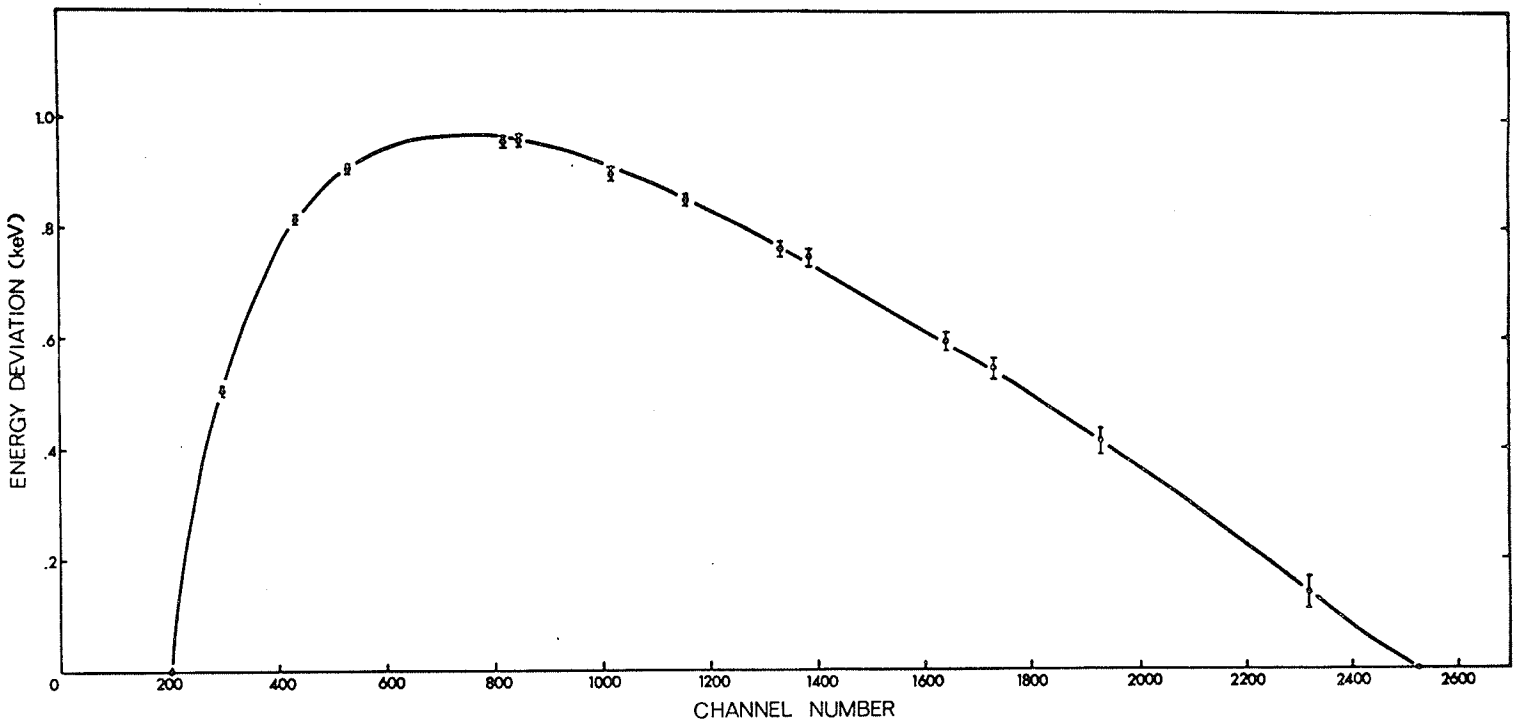
ENERGY DEVIATION (keV)
1.0
.8
.6
.4
.2
0
200
400
600
800
1000
1200
1400
1600
1800
2000
2200
2400
2600
CHANNEL NUMBER

In this particular example, the non-linearity is quite extreme. Had amplifiers of superior quality been used, the deviation from linearity would have been much less than that shown.

For any non-linearity curve, it is important to have as many calibration lines as possible, particularly in the low energy region where the non-linearity is most pronounced. However, for the case of uranium-233, the complex gamma ray spectra made it difficult to use a large number of calibration sources, because the composite spectra became so cluttered that identification of the calibration lines became extremely difficult.

Once the non-linearity curve is drawn, it is used to determine the energy corrections for the unknown photopeaks which can then be added to the calculated energies to give the correct photopeak energy. In this way, calibration runs were used to determine the energies of the more prominent ^{233}U lines, which were then used in subsequent singles experiments as internal calibration lines in the same way that the well known calibration lines were used in the original calibration runs.

II. INTENSITY CALIBRATION

In addition to determining accurately the photopeak energies of an isotope, it is also necessary to determine the intensities of the photopeaks. This involves an efficiency calibration of the detector. If semiconductor detectors were 100% efficient, they would detect every gamma ray emitted by a radioactive source and the intensity of a photopeak would be proportional to the area under the photopeak minus the background contributions. In practice, the efficiency of Ge(Li) and Si(Li) detectors is a function of the source-to-detector (STD) distance, which is a measure of the solid angle subtended by the source at the detector and also a function of the photopeak energy.

The absolute efficiency of a detector is the ratio of the number of gamma rays in the photopeak detected by the detector to the number of gamma rays emitted in all directions in space. Absolute efficiency calibrations are obtained for a particular source-to-detector distance.

For an efficiency calibration, sources with photopeaks of known intensities are used (see Table IV).[12,15,16] In order to make such a calibration, it is necessary to know the strength of the source at the time the experiment is performed. The duration of any experiment is usually negligible with respect to the half-life of the isotope, so the source strength is assumed to be constant while the calibration is being performed. The number of gamma rays

TABLE IV

INTENSITY CALIBRATION STANDARDS

Isotope	Energy (keV)	Photons Per 100 Disintigrations
Am-241	11.9 ± 0.1	0.86 ± 0.03
	13.9 ± 0.1	13.4 ± 0.3
	17.8 ± 0.1	19.5 ± 0.8
	20.8 ± 0.1	4.8 ± 0.3
	26.345 ± 0.001	2.4 ± 0.1
	59.537 ± 0.001	35.9 ± 0.6
Ba-133	53.155 ± 0.016	2.20 ± 0.03
	79.621 ± 0.011	2.4 ± 0.1
	80.997 ± 0.005	32.8 ± 0.6
	160.60 ± 0.04	0.72 ± 0.03
	223.11 ± 0.04	0.47 ± 0.01
	276.397 ± 0.012	7.3 ± 0.1
	302.851 ± 0.015	18.6 ± 0.2
	356.005 ± 0.017	62.27
	383.851 ± 0.020	8.8 ± 0.1
Co-57	122.061 ± 0.010	85.0 ± 1.7
	136.471 ± 0.010	11.4 ± 1.3
Co-60	1173.23 ± 0.04	99.74 ± 0.05
	1332.49 ± 0.05	99.85 ± 0.03
Cs-137	611.635 ± 0.076	85.1 ± 0.4
Mn-54	834.81 ± 0.03	100
Na-22	511.006 ± 0.002	179.7 ± 0.8
	1274.55 ± 0.04	99.95 ± 0.02

emitted by the source in all directions in space is determined from the initial source strength at the time of the experiment and the known intensities of the standard gamma rays. The photopeak area which is obtained from CUTIPIE gives the total number of genuine counts under the photopeak, which is the number of gamma rays detected by the detector. For each gamma ray, the ratio of the total number of gammas detected to the total number emitted is the absolute efficiency of the detector for each particular energy and for the particular source-to-detector distance that was used. By obtaining these ratios for several different energy gamma rays, an efficiency curve can be plotted (see Figures 4,5). If all of the efficiency values are normalized relative to one of the values, then the resulting curve is a relative efficiency curve which is substantially independent of the source-to-detector distance.

The absolute intensities of the gamma rays under study are obtained by taking the ratio of their photopeak areas to the absolute efficiency for their particular energies. In order to use efficiency values from the absolute efficiency curve, all experiments must be performed at the same source-to-detector distance as the calibration work. If relative intensities are all that is required which is normally the case the source-to-detector distance is not an important factor, provided it is not too small.

FIGURE 4

ORTEC Ge(Li) X-RAY DETECTOR EFFICIENCY CURVE

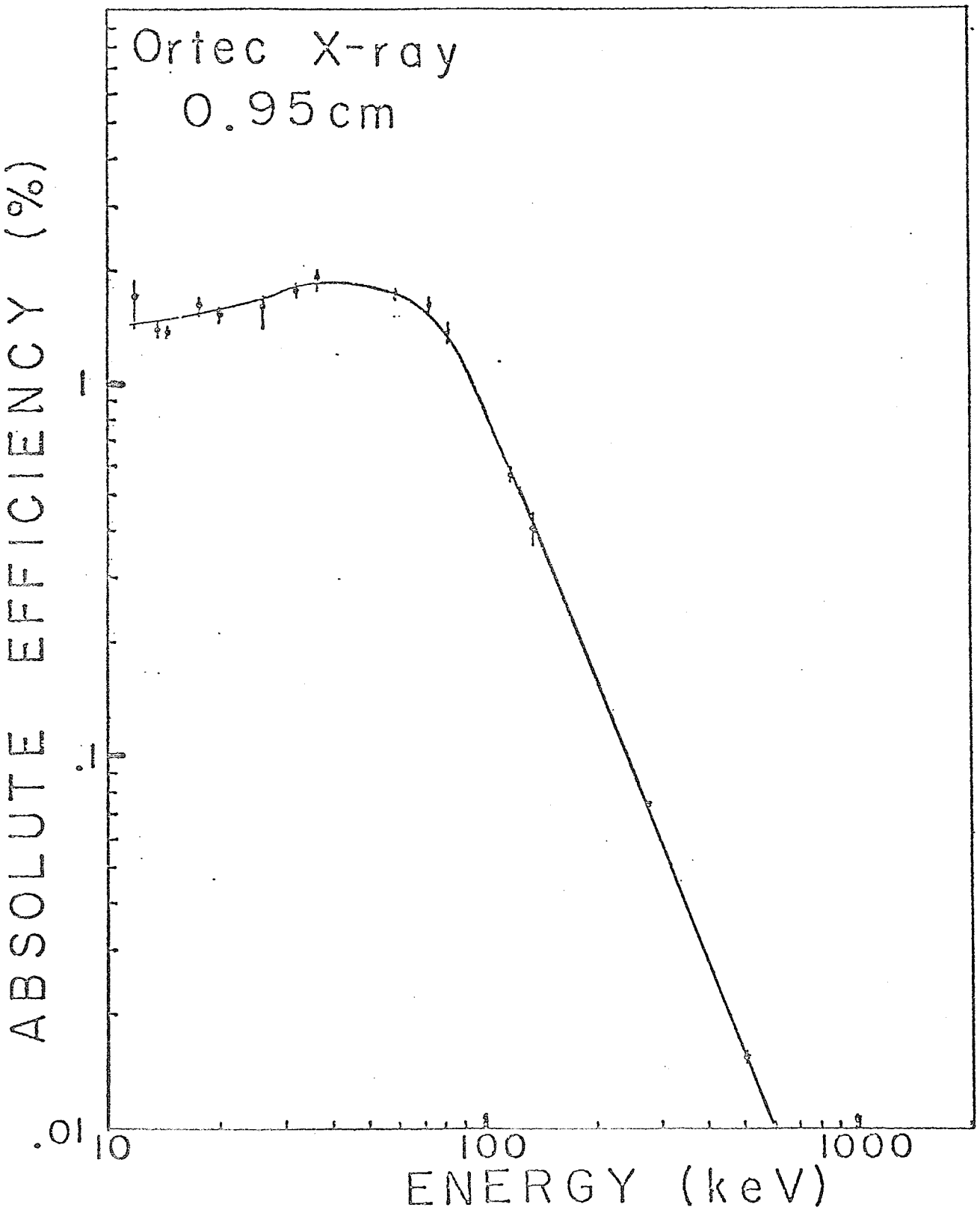
Ortec X-ray
0.95cm
ABSOLUTE EFFICIENCY (%)
1
.1
.01
10
100
1000
ENERGY (keV)

FIGURE 5

50 cc Ge(Li) DETECTOR EFFICIENCY CURVE

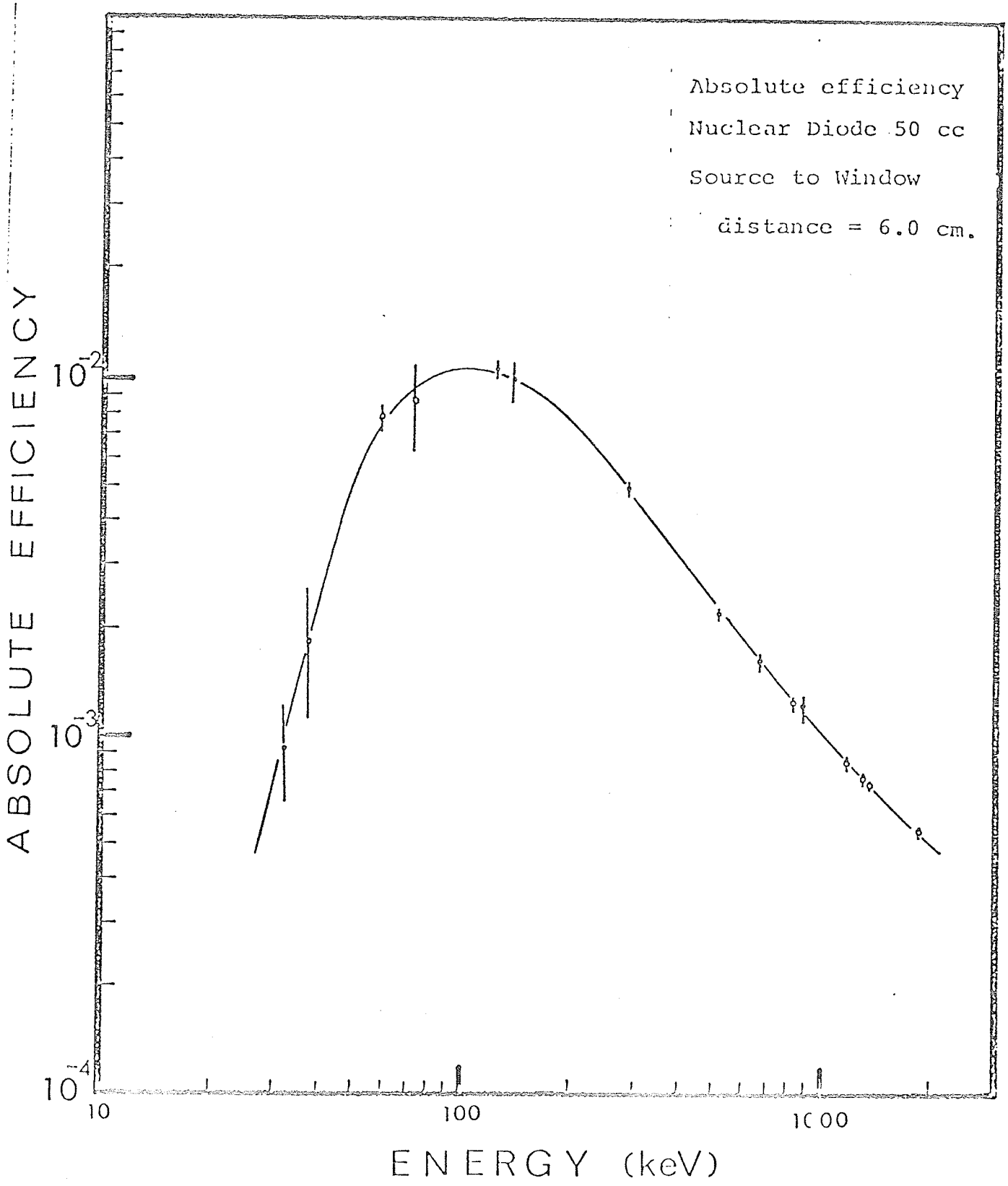
Absolute efficiency
Nuclear Diode 50 cc
Source to Window
distance = 6.0 cm.
ABSOLUTE EFFICIENCY
10^{-2}
10^{-3}
10^{-4}
10
100
1000
ENERGY (keV)

CHAPTER IV

ENERGIES AND INTENSITIES

I. ABSORBERS

Complex gamma ray spectra often appear even more complex than they really are due to the occurrence of sum peaks. These peaks occur when two gamma rays are received by the detector within its resolving time. These two pulses are not recognized as such, but appear as a single pulse and will produce a peak in the gamma ray spectrum at an energy corresponding to that of the sum of the two gamma rays but slightly wider than the peaks corresponding to the two original pulses. This is known as the sum peak. The extra width in the sum peak is due to the various slight differences in the times of entry of the two gamma rays. The probability of the occurrence of sum peaks is proportional to the intensities of the gamma rays involved, so either one or both of the gamma rays are necessarily strong.

This problem occurs often in the study of the heavy elements, because of the strength of their X-rays which are very intense and sum not only with high intensity gamma rays, but also with themselves. By carefully selecting absorbers, it is possible to alleviate this problem and verify that photopeaks are genuine and that their intensities are the actual intensities and not the composite intensity of more than one photopeak.

Gamma rays are attenuated as they pass through

matter and this attenuation is a function of energy. The degree of attenuation caused by any absorber must be taken into consideration when the intensities of gamma rays are determined. This is done by using the exponential decay law:

$$I = I_o e^{-\mu x}$$

where I_o is the original intensity, i.e. the intensity without the absorber, I is the final intensity, i.e. the intensity with the absorber, x is the thickness of the absorber in g/cm^2 and μ is the mass absorption coefficient in cm^2/g.

Since intensity is the ratio of the photopeak area to the efficiency, $I = I_o e^{-\mu x}$ can be replaced by $A = A_o e^{-\mu x}$ where A_o is the area obtained without the absorber and A is the area obtained with the absorber. Hence, the area without the absorber is $A_o = Ae^{\mu x}$. The various areas, A, are obtained from the CUTIPIE analysis of the data. The value of the mass absorption coefficient μ for a particular energy is obtained from the attenuation curve for the particular absorber being used (see Figures 6,7).[17,18] The thickness of the absorber, x, is a constant for each absorber. Thus, using $A_o = Ae^{\mu x}$, the attenuated areas of photopeaks can be corrected to give the true photopeak area and hence intensity which would have been obtained if the absorber hadn't been used.

In the present work, three different absorbers

FIGURE 6

ATTENUATION CURVE OF A Ge FILTER

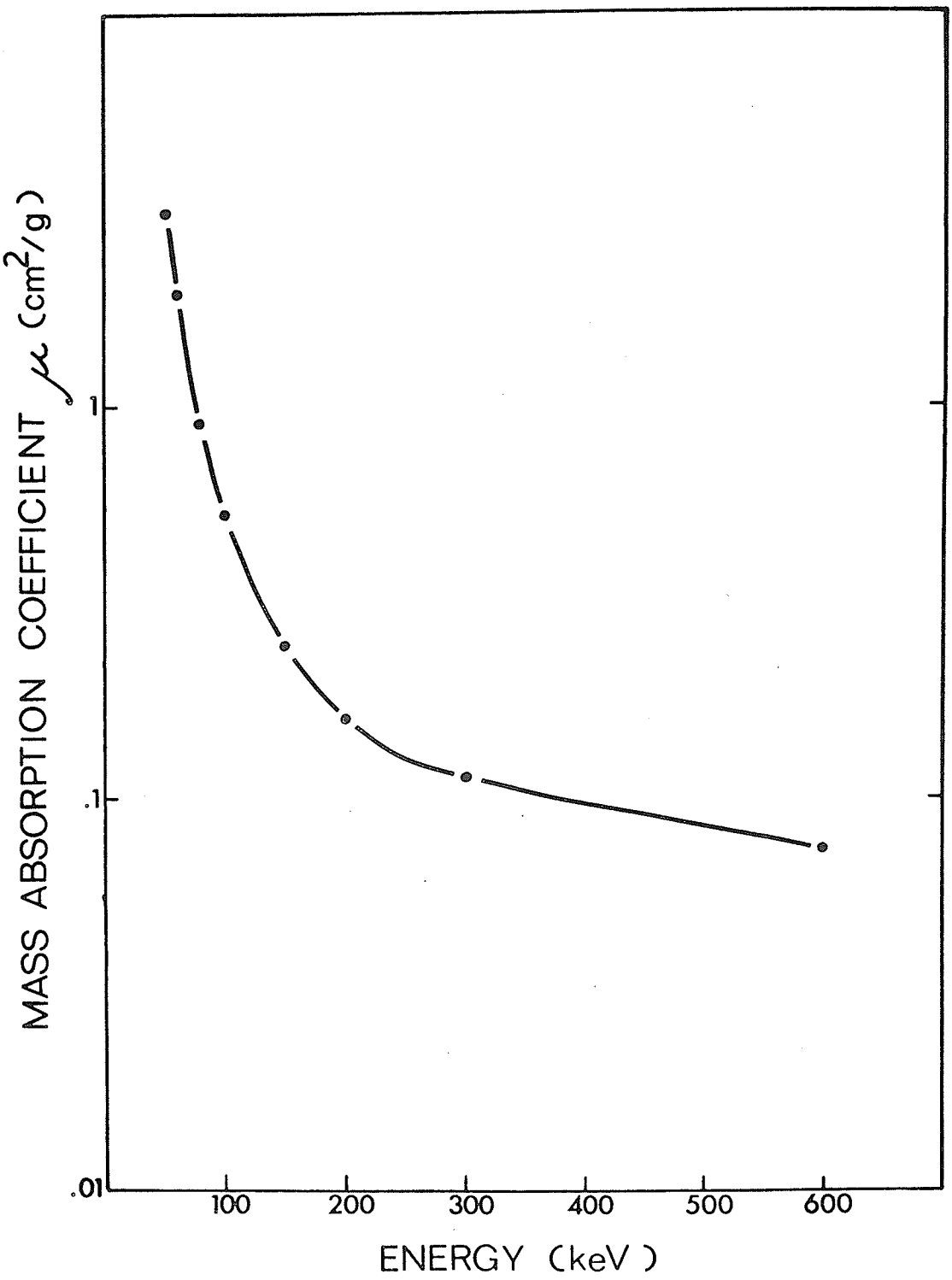
MASS ABSORPTION COEFFICIENT μ (cm²/g)
1
.1
.01
100
200
300
400
500
600
ENERGY (keV)

FIGURE 7

ATTENUATION CURVE OF A Pb FILTER

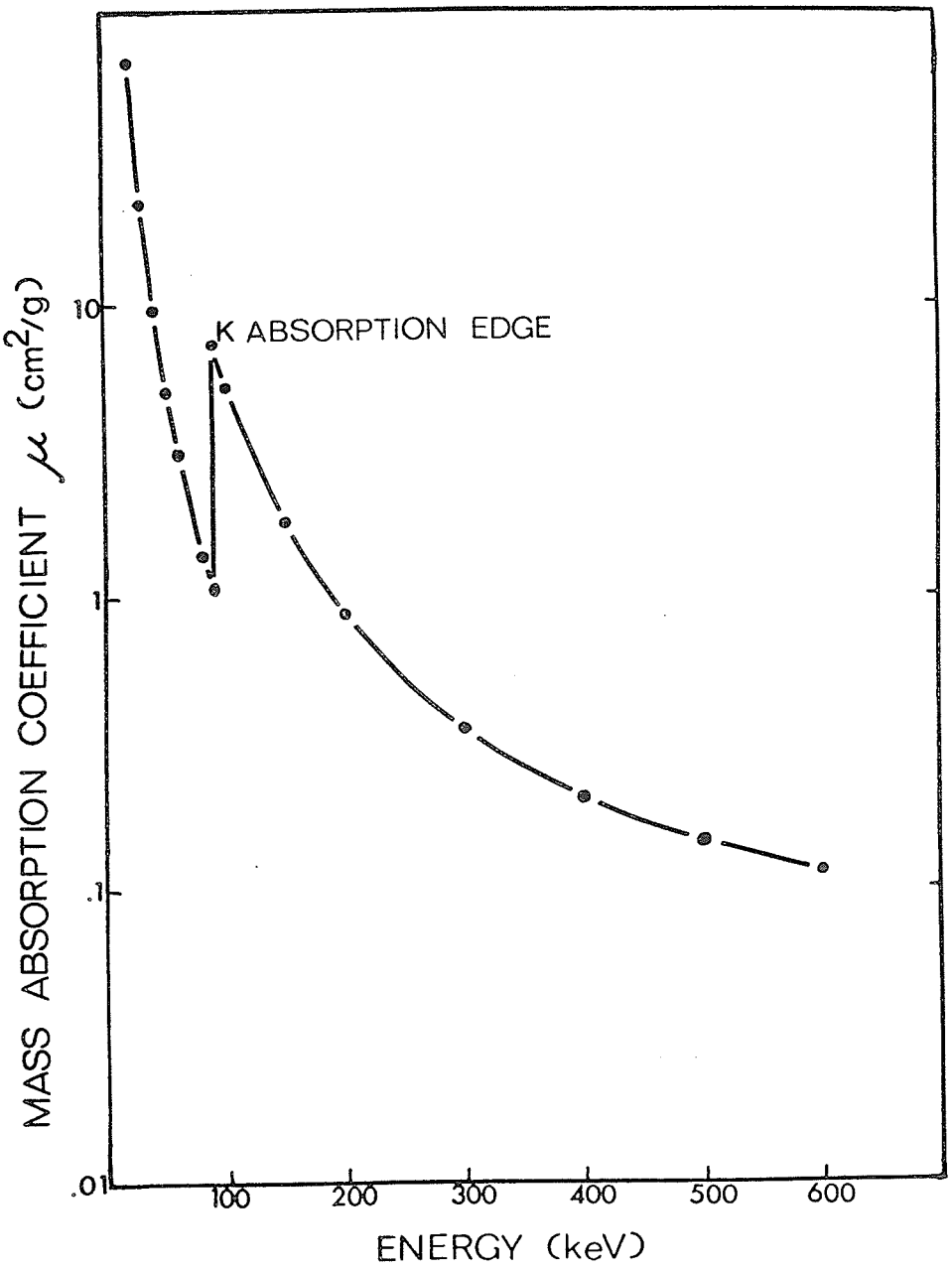
MASS ABSORPTION COEFFICIENT μ (cm^2/g)
10
1
.1
.01
K ABSORPTION EDGE
100
200
300
400
500
600
ENERGY (keV)

were used. To simplify low energy U-233 spectra a Ge filter of 0.130g/cm^2 was used. The K absorption edge of germanium is at 11.104 keV so it effectively eliminates the intense L X-rays from heavy elements. A Pb absorber of 0.7718g/cm^2 whose K absorption edge is about 90 keV was used to attenuate the K X-rays of heavy elements which lie in the region 90 to 115 keV. The K absorption edge of Sn is approximately 25 keV so Sn will not specifically attenuate X-rays, but will cause a general attenuation, particularly at low energies so a Sn absorber of 0.1362 g/cm^2 was also used to compare with the results obtained from the other absorbers.

The corrected areas A_o obtained from the runs with the Sn and Pb absorbers were compared with the areas obtained in a run where no absorber had been used. This comparison allows for the observation of sum peaks, because if they were present in the absorber-free run, their intensities would be greatly reduced in the runs with the absorbers. No summing was observed indicating that all of the observed photopeaks were in fact genuine. That this was so can be attributed to three effects:

(a) relatively weak source strengths;

(b) relatively large source-to-detector distances;

(c) a relatively short resolving time for the detector and associated electronics.

II. ENERGIES AND INTENSITIES

The gamma ray spectrum following the decay of U-233 to Th-229 is extremely complicated. Indeed it has proved to be one of the most complex known. In addition to the 114 gamma rays that were identified, X-rays of thorium and uranium were also observed. Also the U-233 sources which were purchased in 50 milligram (500 μCi) quantities from Amersham Searle Corporation, The Radiochemical Centre, Amersham, Buckinghamshire, England were found to contain small quantities of U-232 and U-234 which could not be removed by purification procedures. These additional uranium isotopes together with the U-233 further complicated the spectra with the gamma rays of their daughters which gradually grew in.

The thorium and radium impurities were removed from U-233 using an ion exchange column. U-233 is strongly adsorbed from HCl solution onto analytical grade anion exchange resin, Bio-Rad AG 1-X8 50-100 mesh, chloride form. This adsorption is a function of HCl molarity, i.e. the higher the acid concentration, the more strongly is the U-233 held onto the resin beads.[19] While the U-233 was held the Th and Ra were washed out. The U-233 was then eluted by washing out with doubly distilled H_2O and the eluant was then boiled down to a small volume to concentrate the source material.

The U-233 in solution was then evaporated to dryness

and covered with several layers of mylar for safety and mounted on either a lucite slide or on a circular metal ring. The source was found to be hygroscopic so it was kept in a desiccator at all times when not in use.

Energy calibration of the uranium gamma rays was performed using the mixed source technique discussed earlier. The uranium source was placed in front of a detector along with one or more calibration sources and a spectrum was accumulated. A non-linearity curve was then drawn so that the stronger U-233 lines could be calibrated with respect to energy. In subsequent calibrations, these lines served as internal calibrations for the weaker lines. This process was repeated several times using different calibration sources and different detectors. The results obtained in the present work are tabulated in Table V along with those of Cline and Kroger. All gamma ray intensities, including those of Cline and Kroger were normalized relative the 208.17 keV gamma ray whose intensity was chosen to be 100. Unless otherwise stated the errors in the intensities of the present work may be taken to be less than 15%.

Figures 8 and 9 show the gamma ray spectrum of U-233 for the energy region less than 60 keV. These two spectra illustrate the superior resolving power of the Si(Li) detector to that of the Ge(Li) detector in the energy region below 40 keV. The spectrum shown in Figure 8 was taken with the KEVEX Si(Li) X-ray detector at a STD dis-

TABLE V

ENERGIES AND INTENSITIES

\# Linking Transitions

* Coincidence Data Only (Present Work)

C.D. Coincidence Data Only (Kroger)

CLINE		KROGER		PRESENT WORK	
ENERGY (keV)	INTEN-SITY	ENERGY (keV)	INTEN-SITY	ENERGY (keV)	INTEN-SITY
				14.44#	
		25.30±0.06	100.0	25.27±0.12	48.5
				27.33#	
29.000±0.100	532.4	29.16±0.06	500.0	29.15±0.09	272.2
				29.36*	
				31.52±0.04	10.8
		32.2 ±0.2	—	32.48±0.15	39.6
		37.8 ±0.1	20.8	37.98±0.12	14.2
42.400±0.100	2779.4	42.44±0.02	2583.3	42.48±0.03	2412.2
				42.69*	
				50.42*	
		52.6 C.D.		52.62*	
54.690±0.100	608.8	54.69±0.02	625.0	54.74±0.05	559.8
		63.88±0.15	1.3	63.7*	
		65.7 C.D.		65.33*	
66.140±0.050	30.9	66.11±0.04	36.3	66.13±0.05	33.8
68.030±0.050	10.3	67.98±0.05	8.3	68.08±0.01	12.7
				68.87±0.05	4.3
70.370±0.050	23.5	70.33±0.05	24.6	70.30±0.05	23.8
71.880±0.050	123.5	71.84±0.02	120.8	71.84±0.04	106.3±8.9
				72.88±0.07	23.5
74.960±0.050	64.7	74.59±0.05	66.7	74.55±0.00(1)	49.3±1.8
				74.86±0.00(8)	16.3±1.6
76.410±0.050	23.5	76.41±0.08	21.7	76.38±0.00(7)	15.6±0.8
				76.98#	
				77.13±0.04	28.7±3.2
77.860±0.100	13.2	78.20±0.10	4.2	78.09±0.14	2.4
83.060±0.050	5.9	83.08±0.05	5.8	83.00±0.02	7.2±0.4
85.23 ±0.15	1.5			85.43±0.02	7.6±1.7
				86.77±0.15	5.4
				87.27±0.11	7.5
				88.46±0.08	17.6±0.0(3)
90.500±0.300	13.2	91.0 ±0.5	8.3	91.03±0.01	13.2±0.0(3)
96.26 ±0.12	—	96.28±0.10	125.0	96.21±0.04	55.4±2.6
97.210±0.100	883.8	97.14±0.02	916.7	97.14±0.05	886.7±45.8
100.030±0.120	1.5	100.03±0.15	2.1	100.03±0.02	2.2
101.770±0.100	2.9	101.75±0.10	2.9	101.77±0.07	3.6
		103.4 C.D.		103.71±0.03	4.0
109.520±0.100	14.7	109.5 ±0.1	12.5		
112.010±0.100	19.1	112.0 ±0.1	18.8		
		114.4 C.D.			
				116.41±0.07	8.5
117.220±0.050	126.5	117.16±0.02	108.3	117.18±0.03	99.6±2.2
119.010±0.050	158.8	118.98±0.02	154.2	118.98±0.04	127.1±2.5
120.830±0.050	130.9	120.82±0.05	129.2	120.82±0.00(5)	82.2±0.8
123.920±0.060	30.9	123.93±0.05	30.4	123.88±0.02	25.9±2.0
125.480±0.100	4.4	125.4 ±0.1	2.9	125.41±0.06	2.6
				128.31*	

CLINE		KROGER		PRESENT WORK	
ENERGY (keV)	INTEN-SITY	ENERGY (KeV)	INTEN-SITY	ENERGY (keV)	INTEN-SITY
129.28 ±0.05	—	129.4 ±0.1	4.2	129.10±0.03	2.8
131.050±0.120	2.9	131.05±0.15	1.3	131.34±0.11	1.3±0.2
135.350±0.050	94.1	135.34±0.05	95.8	135.37±0.03	87.0±3.8
				138.5#	
139.780±0.050	4.4	139.72±0.08	4.2	139.79±0.06	4.2±0.5
		141.6 C.D.			
		144.7 ±0.5	37.5	144.32±0.08	11.8±2.6
145.350±0.120	76.5	145.37±0.1	62.5	145.34±0.04	66.0±11.2
146.380±0.060	270.6	146.34±0.05	266.7	146.39±0.03	251.4±12.8
148.260±0.120	14.7	148.14±0.05	17.5	148.20±0.05	14.4±2.6
149.760±0.120	4.4	149.86±0.1	5.4	149.83±0.12	5.1±0.1
153.440±0.130	4.4	153.2 ±0.2	5.8	153.05±0.11	2.2±0.1
154.980±0.130	7.4	154.85±0.1	7.1	154.69±0.12	6.0±0.7
156.210±0.130	2.9	156.1 ±0.15	2.9	156.14±0.16	2.3±0.3
162.570±0.130	5.9	162.6 ±0.1	10.0	162.27±0.14	3.0±0.9
164.600±0.050	260.3	164.53±0.03	258.3	164.54±0.01	266.1±11.2
165.630±0.130	20.6	165.6 ±0.1	18.8	165.72±0.10	15.4±2.8
169.030±0.130	4.4	168.96±0.10	4.2	169.05±0.05	2.7±0.7
170.820±0.080	7.4	170.84±0.05	8.3	170.84±0.05	5.6±0.8
172.52 ±0.15	—	172.42±0.12	1.3	172.30±0.16	1.35
174.180±0.060	13.2	174.17±0.05	11.7	174.21±0.03	9.3±1.5
				176.13±0.07	1.7±0.6
				177.81±0.06	0.8±0.1
184.39 ±0.10	—	184.4 ±0.1	5.8	184.21±0.29	1.0
				185.81±0.02	1.6±0.1
187.970±0.050	82.4	187.96±0.02	83.3	187.97±0.01	81.6±1.2
192.140±0.060	4.4	192.13±0.08	2.9	192.13±0.04	1.6±0.2
		200.7 ±0.1	0.04		
206.050±0.140	2.9	206.2 ±0.2	4.2	205.98±0.12	2.6
208.180±0.050	100	208.18±0.05	100	208.17±0.02	100
212.370±0.050	4.4	212.36±0.05	4.2	212.32±0.08	5.5±0.3
216.500±0.300	38.2	216.1 ±0.2	33.3	216.08±0.02	26.5±4.2
217.130±0.050	120.6	217.15±0.05	145.8	217.13±0.04	142.7±1.8
219.360±0.080	7.4	219.42±0.10	7.1	219.34±0.04	6.0±0.5
223.450±0.080	1.5	223.45±0.10	1.3	223.17±0.04	1.3±0.1
		224.8 ±0.1	1.2	225.00±0.30	0.4
				226.72±0.28	0.4
		228.1 ±0.1	0.8		
230.120±0.080	4.4	230.11±0.05	3.3	230.11±0.02	2.7±0.3
		236.3 ±0.1	0.4	236.42±0.21	2.0
240.370±0.080	13.2	240.35±0.05	12.9	240.43±0.04	15.2±1.5
245.340±0.050	157.4	245.33±0.03	158.3	245.32±0.02	158.5±4.1
248.730±0.050	63.2	248.71±0.04	62.5	248.69±0.03	62.5±2.5
				252.53±0.11	1.5±0.1
255.940±0.100	2.9	255.93±0.05	1.3	255.95±0.04	1.7±0.2
259.380±0.080	8.8	259.36±0.05	8.8	259.33±0.04	7.1±0.7
				260.65±0.22	4.3±0.3
261.92 ±0.08	13.2	261.92±0.05	13.3	261.91±0.09	12.4±0.9

CLINE		KROGER		PRESENT WORK	
ENERGY (keV)	INTEN-SITY	ENERGY (keV)	INTEN-SITY	ENERGY (keV)	INTEN-SITY
268.680±0.050	11.8	268.67±0.05	10.8	268.66±0.03	10.2±0.9
272.350±0.060	4.4	272.36±0.05	5.0	272.31±0.08	2.5±0.3
274.710±0.050	20.6	274.71±0.04	20.0	274.68±0.05	17.4±0.4
278.100±0.050	47.1	278.10±0.04	50.0	278.08±0.02	47.1±1.1
		284.25±0.15	0.4		
288.030±0.050	39.7	288.01±0.04	37.5	288.00±0.03	42.4±4.3
291.340±0.050	235.3	291.34±0.03	229.2	291.34±0.01	230.1±0.8
294.030±0.080	5.9	293.94±0.10	7.1	293.89±0.04	5.6±0.5
				295.17±0.48	0.9±0.2
303.010±0.080	4.4	302.96±0.05	3.8	302.81±0.19	2.8±0.8
309.530±0.100	4.4	309.49±0.10	4.2	309.76±0.08	4.3±0.2
317.150±0.050	339.7	317.15±0.02	333.3	317.16±0.01	326.8±2.4
320.540±0.050	127.9	320.53±0.03	125.0	320.54±0.01	121.1±1.1
323.360±0.050	36.8	323.37±0.04	36.3	323.47±0.26	33.8±0.7
328.720±0.060	4.4	328.74±0.05	2.8	328.50±0.19	2.6±0.5
336.600±0.050	25.0	336.60±0.04	24.6	336.62±0.02	23.7±0.3
				351.81±0.01	1.8±0.3
354.000±0.150	4.4	354.05±0.05	2.6	354.01±0.01	2.3±0.4
365.790±0.060	36.8	365.79±0.03	36.3	365.79±0.01	32.9±0.7
383.510±0.080	4.4	383.43±0.10	4.2	383.50±0.08	3.8
		393.59±0.10	0.7	393.80±0.10	0.3
		396.7 ±0.1	0.3		
		402.4 ±0.2	0.3		
		406.7 ±0.3	0.2		
		416.4 ±0.2	0.6	416.40±1.20	0.4
		436.6 ±0.4	1.5		
		449.5 ±0.2	0.4	449.63±1.53	0.4
		459.8 ±0.2	0.3		
		471.0 ±0.2	0.8	471.25±1.30	0.62
		478.6 ±0.2	0.8	478.74±2.59	0.60
		484.1 ±0.2	0.2		
		514.0 ±0.5	—		
		537.6 ±0.5	—		
		540.3 ±0.2	0.2		
		545.1 ±0.3	0.1		
		562.8 ±0.5	—		
		569.4 ±0.2	0.2		
		578.5 ±0.2	0.2		
		620.9±±0.2	0.1		
		657.0 ±0.2	0.1		
		707.5 ±0.2	0.1		
		710.8 ±0.5	—		
		826.3 ±0.5	—		
		867.9 ±0.4	0.1		
		920 ±1.0	—		
		1003 ±1.0	0.3		
		1055 ±1.0	—		
		1119 ±1.0	0.3		

FIGURE 8

^{233}U GAMMA RAY SPECTRUM FOR E<60keV

USING A Si(Li) DETECTOR

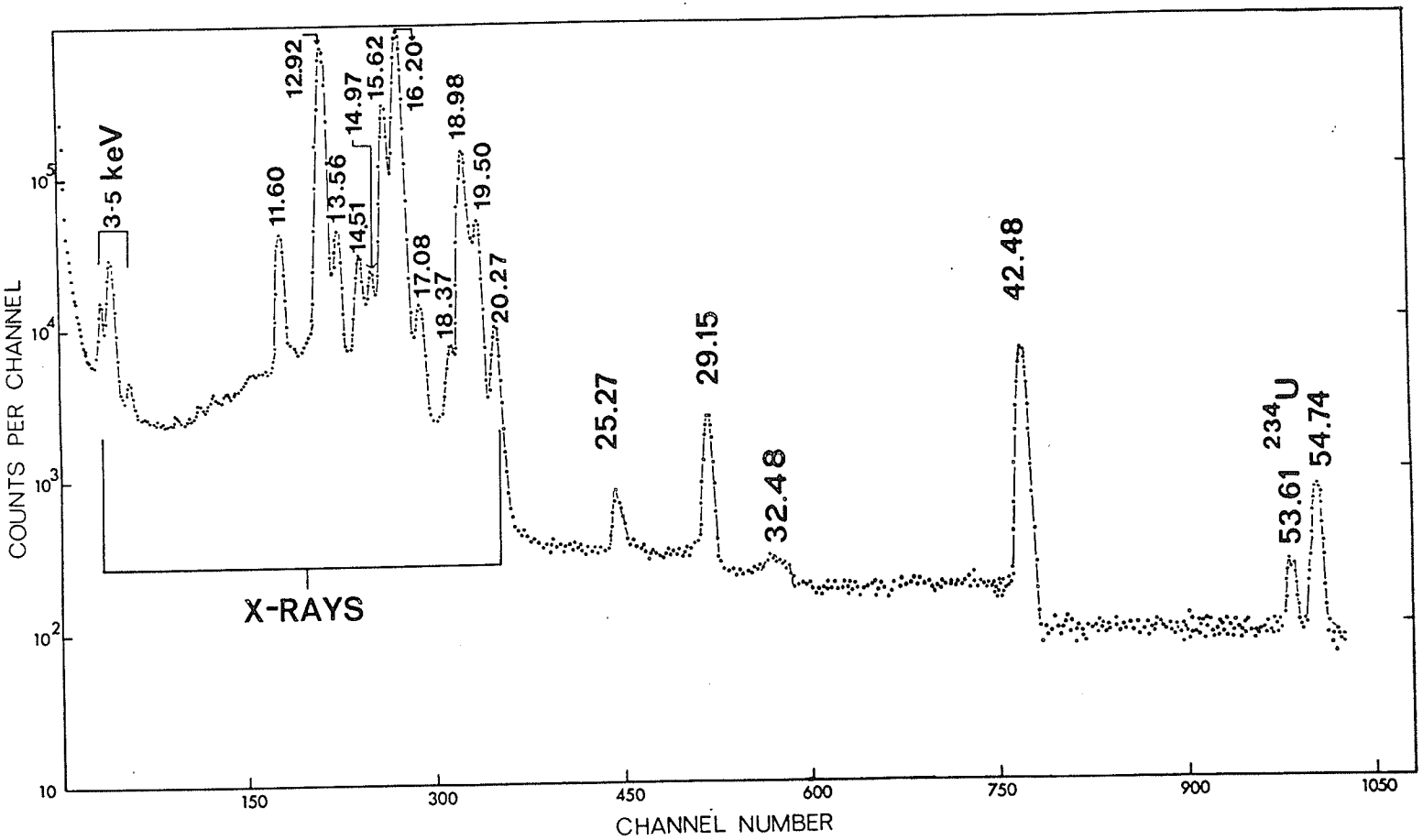
COUNTS PER CHANNEL
CHANNEL NUMBER
X-RAYS
3·5 keV
11.60
12.92
13.56
14.51
14.97
15.62
16.20
17.08
18.37
18.98
19.50
20.27
25.27
29.15
32.48
42.48
53.61
234U
54.74
10
10²
10³
10⁴
10⁵
150
300
450
600
750
900
1050

FIGURE 9

^{233}U GAMMA RAY SPECTRUM FOR E<60keV

USING A Ge(Li) X-RAY DETECTOR

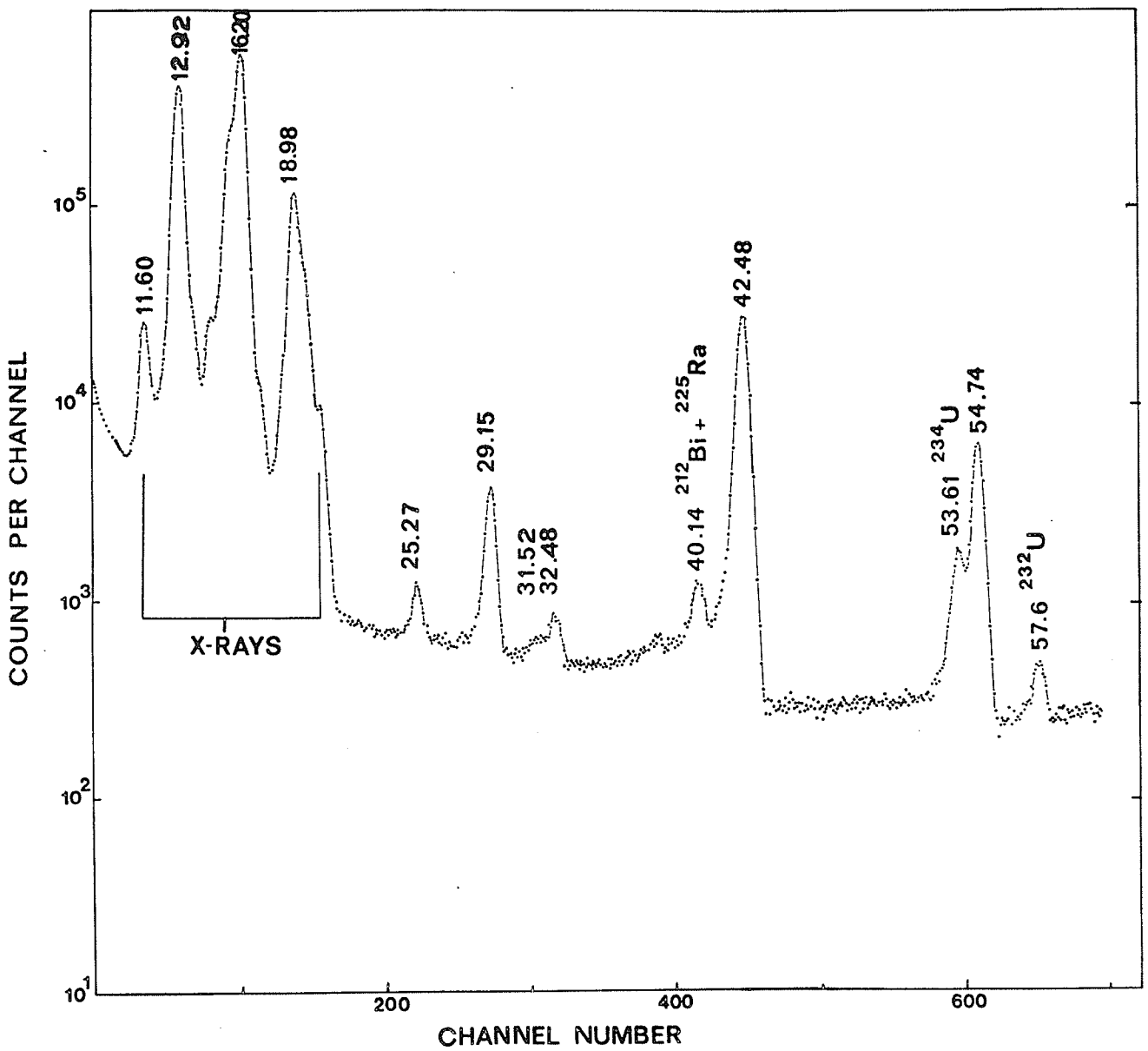
COUNTS PER CHANNEL
CHANNEL NUMBER
X-RAYS
11.60
12.92
16.20
18.98
25.27
29.15
31.52
32.48
40.14 212Bi + 225Ra
42.48
53.61 234U
54.74
57.6 232U
10^5
10^4
10^3
10^2
10^1
200
400
600

tance of 2.5 cm for an accumulation time of 50.8 ks while the ORTEC Ge(Li) X-ray detector #2 at a STD distance of 4.5 cm and an accumulation time of 40 ks yielded the spectrum shown in Figure 9. The complex X-ray region from 11 to 20 keV was resolved into most of its individual components by the high resolution Si(Li) detector, while the unwrapping facilities of CUTIPIE were relied on to obtain the X-ray components in the spectrum taken with the Ge(Li) X-ray detector. The various X-ray components are listed in Table VI. The 40.14 keV and 53.61 keV components in Figure 9 are examples of additional gamma rays resulting from the decay of U-232 and U-234. The 53.61 keV gamma ray comes from U-234, but the 40.14 keV could originate from Ra-225 which is a daughter product of U-233 or from Bi-212 one of the daughters of U-232. The 57.6 keV gamma also comes from U-232. The 40.14 keV gamma and the 57.6 keV gamma are not seen in Figure 8 because the source used for that spectrum had been chemically purified to remove the thorium and radium prior to the experimental run, while an older source was used to obtain the other spectrum.

The ORTEC Ge(Li) X-ray detector #1 was used to obtain the spectrum shown in Figure 10. A Ge filter (0.13g/cm^2) was used to absorb the X-rays from thorium. The U-233 source used for this spectra had not been recently purified prior to the time of the experiment and several lines that appear in the spectra can be attributed to daughter products

FIGURE 10

^{233}U GAMMA RAY SPECTRUM FOR E<230keV

USING A Ge(Li) X-RAY DETECTOR WITH

A Ge FILTER ($0.13 g/cm^2$)

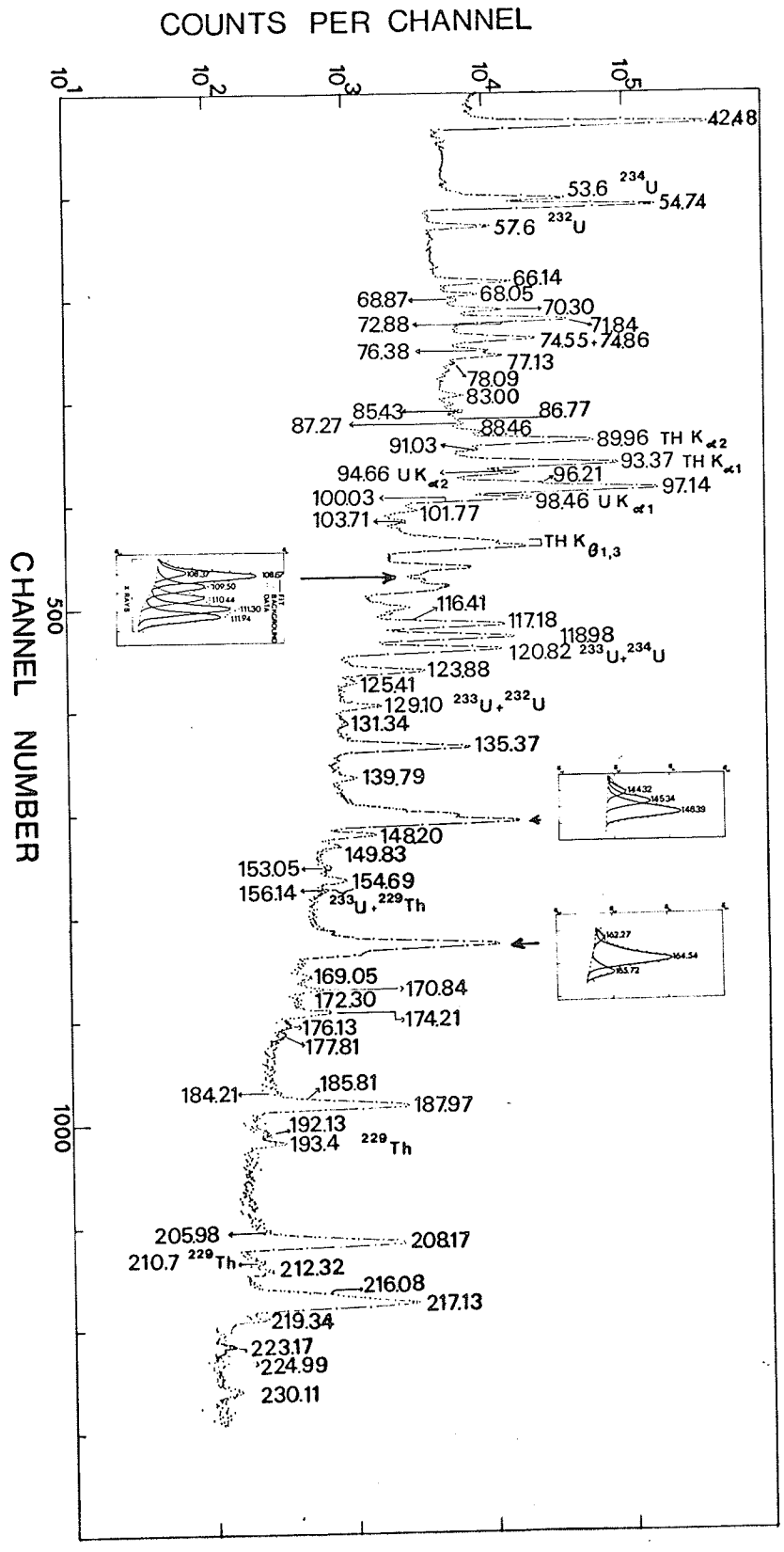
COUNTS PER CHANNEL
10^1
10^2
10^3
10^4
10^5
CHANNEL NUMBER
500
1000
42.48
53.6 234U
54.74
57.6 232U
66.14
68.87
68.05
70.30
72.88
71.84
74.55
74.86
76.38
77.13
78.09
83.00
85.43
86.77
87.27
88.46
91.03
89.96 TH Kα2
93.37 TH Kα1
94.66 U Kα2
96.21
97.14
100.03
98.46 U Kα1
103.71
101.77
TH Kβ1,3
116.41
117.18
118.98
120.82 233U, 234U
123.88
125.41
129.10 233U, 232U
131.34
135.37
139.79
144.32
145.34
146.39
148.20
149.83
153.05
154.69
156.14
233U, 229Th
162.27
164.54
165.72
169.05
170.84
172.30
174.21
176.13
177.81
184.21
185.81
187.97
192.13
193.4 229Th
205.98
208.17
210.7 229Th
212.32
216.08
217.13
219.34
223.17
224.99
230.11

TABLE VI

X-RAY COMPONENTS

Energy (keV)	X-ray
11.60	U L_{III}, M_I
12.92	Th L_{α_2} + L_{α_1}
13.56	U L_{α_1} + L_{α_2}
14.51	Th L_n
14.97	Th L_{β_6}
15.62	Th L_{β_3} + L_{β_4}
16.20	Th L_{β_1}
17.08	Th L_{β_9} + $L_{\beta_{10}}$
18.37	Th L_{γ_5}
18.98	Th L_{γ_1}
19.50	Th L_{γ_2} + L_{γ_3} + L_{γ_6}
20.27	Th L_{γ_4}

and are labelled as such in the figure. The energies of the gamma rays determined in the present work are in good agreement with those of Cline and Kroger where comparable data exists. Many of the differences which appear in the photopeak intensities are due to our having the ability to resolve overlapping photopeaks. The inserts in this figure show the peaks fitted by CUTIPIE. The first insert identifies the components of the uranium and thorium B X-rays. All of the photopeaks assumed to be X-rays are given in Table VII.

The intensity of the 120.82 keV gamma ray in Table V is considerably smaller than the values reported by Cline and Kroger. The present data suggests that the 120.82 keV gamma ray is not only from U-233 but also from U-234. In comparing the intensities of the 120.82 keV gamma ray to that of the 53.61 keV gamma ray, both of which are known to be in the U-234 decay, it was found that the ratio I_{53}/I_{120} was much smaller than that predicted by the intensities found in the Nuclear Data Sheets for U-234. This indicated that the intensity of the 120.82 keV gamma was larger than it should be, which suggested the possibility of two photopeaks superimposed on one another. By reducing the total intensity observed in the present work by a suitable factor necessary to compensate for the U-234 contribution, the intensity of the 120.82 keV gamma ray from the decay of U-233 was obtained and this value is that quoted in Table V.

TABLE VII

X-RAY COMPONENTS

Energy (keV)	X-ray
89.96	Th K_{α_2}
93.37	Th K_{α_1}
94.66	U K_{α_2}
98.46	U K_{α_1}
104.83	Th K_{β_3}
105.63	Th K_{β_1}
108.37	Th $K_{\beta_2^{II}}$
108.67	Th $K_{\beta_2^{I}}$
109.50	Th K $O_{II, III}$
110.44	U K_{β_3}
111.31	U K_{β_1}
111.94	U K_{β_5} (?)
114.49	U $K_{\beta_2^{I}}$ + $K_{\beta_2^{II}}$
115.34	U K $O_{II,III}$

By using a similar line of reasoning, the intensity value that is reported for the 129.10 keV gamma ray is smaller than that given by Cline and Kroger. By comparing the intensity ratios of the 57.6 keV gamma from U-232 and the 129.10 keV gamma with the accepted values a discrepancy again arises indicating that along with U-233, U-232 was also contributing to the intensity of the gamma ray. The corrected intensity value is given in Table V. The intensities of the 144.32, 145.34 and 146.39 keV gamma rays vary from those given by Cline and Kroger, but the total intensity of the three peaks is comparable for each of the three sets of data as is shown in Table V. The new 144.32 keV gamma ray was also placed in the decay scheme. The intensities of the 154.69 and 156.14 keV gamma rays are less than those given by Cline and Kroger, because as with the 120.82 and 129.10 keV gamma rays, it appears as if more than one gamma ray is contributing to the photopeak intensity. The daughter of U-233, Th-229 has four gamma rays which interfere with our spectrum at 154, 156, 193 and 210 keV. All are labelled in the figure and the intensities listed for the 154.69 and 156.14 keV gamma rays have been corrected to compensate for this. The difference in intensities in the 162.27, 164.54 and 165.72 keV group is also explained by the peak fitting process, because the total intensity agrees well with the totals as given by Cline and Kroger (see Table V).

Figure 11 shows a U-233 spectrum for the energy

FIGURE 11

^{233}U GAMMA RAY SPECTRUM FOR 200 keV<E<600 keV

USING A 52 cc Ge(Li) DETECTOR

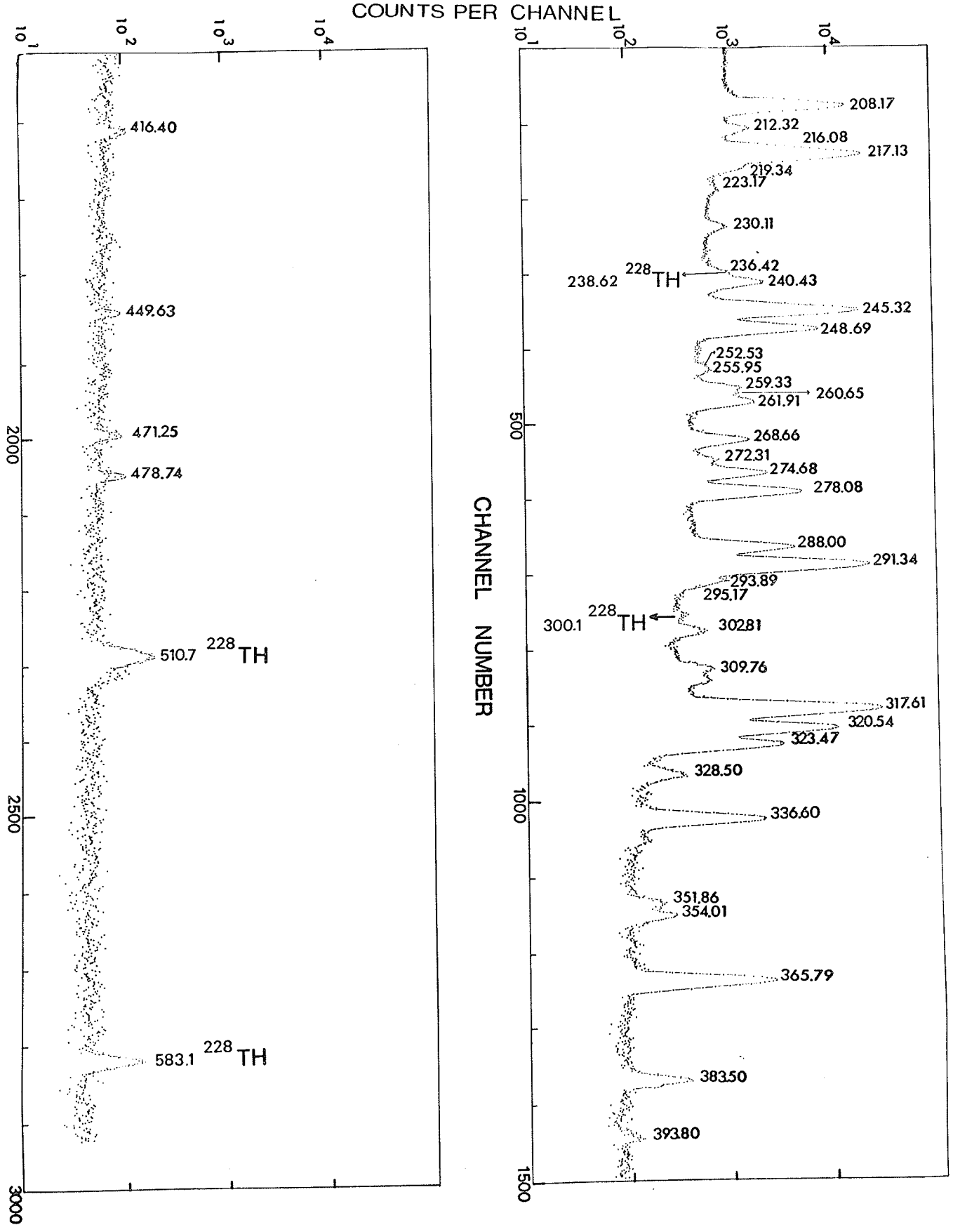
COUNTS PER CHANNEL
CHANNEL NUMBER
416.40
449.63
471.25
478.74
510.7 228TH
583.1 228TH
208.17
212.32
216.08
217.13
219.34
223.17
230.11
236.42
238.62 228TH
240.43
245.32
248.69
252.53
255.95
259.33
261.91
260.65
268.66
272.31
274.68
278.08
288.00
291.34
293.89
295.17
300.1 228TH
302.81
309.76
317.61
320.54
323.47
328.50
336.60
351.86
354.01
365.79
383.50
393.80

region 200-600 keV taken with the ORTEC. 52 cc Ge(Li) detector. As before, any lines belonging to daughter products are labelled. Some discrepancies arise between the gamma rays proposed by Kroger in the energy region beyond 365 keV and the results of the present work. According to Kroger, the gamma ray whose energy is 416.40 keV should be approximately one third as intense as the 383.43 keV gamma ray and so would be clearly seen. However, such a peak is only barely visible in the present work and as an upper limit to the intensity the present work indicates a ratio of one tenth. Kroger gives the same intensity for the 471.25 and 478.74 keV gamma rays while the present work shows the intensity of the 478.74 keV gamma ray to be somewhat less than that for the 471.25 keV gamma ray. Further, if Kroger's intensity values are correct, his gamma ray of 436.6 keV should be clearly visible and approximately $2\frac{1}{2}$ times as intense as the 416.40 keV gamma, but it is not seen in the present work.

For the energy region of 400 to 1119 keV Kroger is sufficiently unsure of the identification of 26 photopeaks that he states in his thesis "The origin of the following gamma rays is less certain." Other than the gamma rays of energies 416.40, 449.63, 471.25 and 478.74 keV, the present work gives no evidence to support the other 22 gamma rays.

The present work indicates that gamma rays one tenth as intense as the 383.43 keV transition would be seen.

According to Kroger, none of his gamma rays of energy greater than 480 keV are as intense as this, so it cannot be said that the radiations he mentions, but cannot place in the decay scheme, are not present in the decay of U-233. However, some of the gamma rays which he mentions as having energies less than 480 keV are not seen in this work although the intensity which he has assigned to them would have enabled them to have been visible above the background. With the possibility of weak contributions from many daughter products of the uranium isotopes present in all samples of "U-233", difficulty in identification in so rich a spectrum is to be expected.

CHAPTER V

GAMMA-GAMMA COINCIDENCE MEASUREMENTS

I. COINCIDENCE GATES

Gamma-gamma coincidence work has been carried out employing the circuit described in Chapter II. This work enables the construction of a decay scheme or level diagram for Th-229 which is the daughter product of U-233. The levels above the ground state of Th-229 are known as its excited states and they are quantized in energy and angular momentum.

The basic aim of any coincidence work is to observe cascades of gamma rays. Cascades occur when one gamma ray populates an excited state which then de-excites emitting another gamma ray. These two gamma rays are said to be in coincidence. As mentioned earlier, the experimental technique that was used allowed for the simultaneous collection of all coincidence events. During the subsequent analysis of the data, gates were set on particular gamma rays and all gamma rays in coincidence with the gating lines were obtained. It is possible that gamma rays which are not true coincidences may appear in the coincidence spectra and these are known as random events. The random coincidence rate N_R is given by $\tau N_1 N_2$ where τ is the time resolution of the system in seconds and N_1 and N_2 are the counting rates of each of the two detectors. The time resolution at FWHM of the system used in the present work was 24.4 nanoseconds (see Figure 12).

FIGURE 12

TIME RESOLUTION

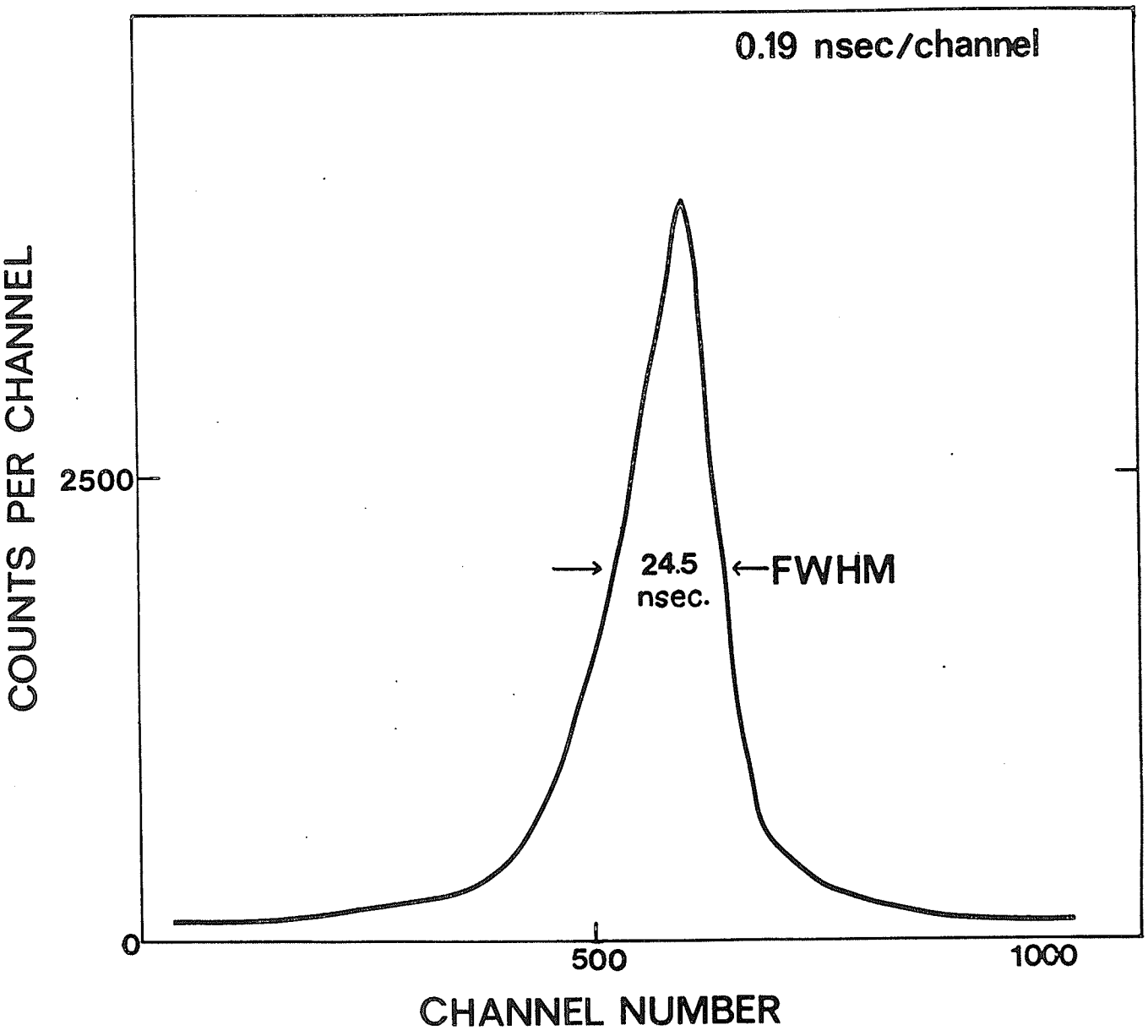
0.19 nsec/channel
COUNTS PER CHANNEL
2500
0
24.5
nsec.
FWHM
500
1000
CHANNEL NUMBER

For analysis, the TAC window width was set at 160 nanoseconds so as to minimize the loss of coincident events. For this resolving time, the random coincidence rate was 2.4 events/sec while the total coincidence rate was 60.0 events/sec so the true to random ratio was 25:1. Random events which appear in coincidence spectra are easily identified because the relative intensities of the gamma rays collected due to random events are in the same ratio as they are in the singles spectra, but they are greatly reduced in intensity.

The source used for the coincidence work was not purified to remove thorium so the gamma rays of daughters of Th-228 are found in the coincidence spectra and are labelled as Th-228. Ten major gamma rays were used as gates in the coincidence measurements. They were the 42.48, 135.37, 139.79, 145.34, 164.54, 208.17, 217,13, 245.32, 278.08, and the 291.34 keV gamma rays. Four of these gamma rays have other gammas in close proximity which are generally weaker so that more than one photopeak was included in some of the gates. The gate set on the 146.39 keV gamma ray also included the 145.34 and 148.20 keV gamma rays and the 162.27 and 165.72 keV gamma rays were included in the gate set on the 164.54 keV gamma ray. Both the 208.17 keV and the 217.13 keV gammas have adjacent weak peaks, viz., 205.98 keV and 216.08 keV and 219.34 keV respectively which would be included in the two gates set on the 208.17 keV gamma ray and the 217.13 keV gamma ray. In discussing the coincidence spectra in

detail it would be helpful to refer to the proposed level scheme (see Figure 21).

42.48 keV Gate:

This is by far the most complicated, but yet the most interesting of the coincidence spectra, because it provides the building blocks for the decay scheme shown in Figure 21. The coincidence spectrum for the 42.48 keV gate is shown in Figure 13. The lines which are enhanced, (all of which are placed in the decay scheme), are the 54.74, 63.7, 66.13, 74.55, 83.00, 120.82, 123.88, 145.34, 216.08, 219.34, 240.43, 245.32, 248.69 and the 278.08 keV gamma rays. The gamma rays whose energies are 74.55, 123.88, 145.34, 216.08, 245.32 and 248.69 keV populate the 71.84 keV level. To get to the 42.48 keV level a 29.36 keV gamma ray link is needed and is observed in the coincidence spectrum. In addition, it may well be that the 42 keV transition is a doublet consisting of the transition to the ground state and also that from the 71.84 to the 29.15 keV levels. This second transition of energy 42.69 keV would probably not be distinguished from the 42.48 keV gamma. This latter transition would account, at least in part, for the presence of gamma rays feeding the 71.84 keV level in this coincidence spectrum. The 29.36 keV transition shown dashed in Figure 21 would also link to the 42 keV level. This would explain the enhancement of the 29 keV peak in the coincidence spectrum. The 54.74, 83.00, 120.82 and 278.08 keV gamma rays feed the 42.48 keV level directly. The X-rays shown in the figure are uranium and thorium K X-rays and also Pb X-rays resulting from the fluorescent excitation

FIGURE 13

COINCIDENCE SPECTRUM WITH THE 42.48 keV LINE

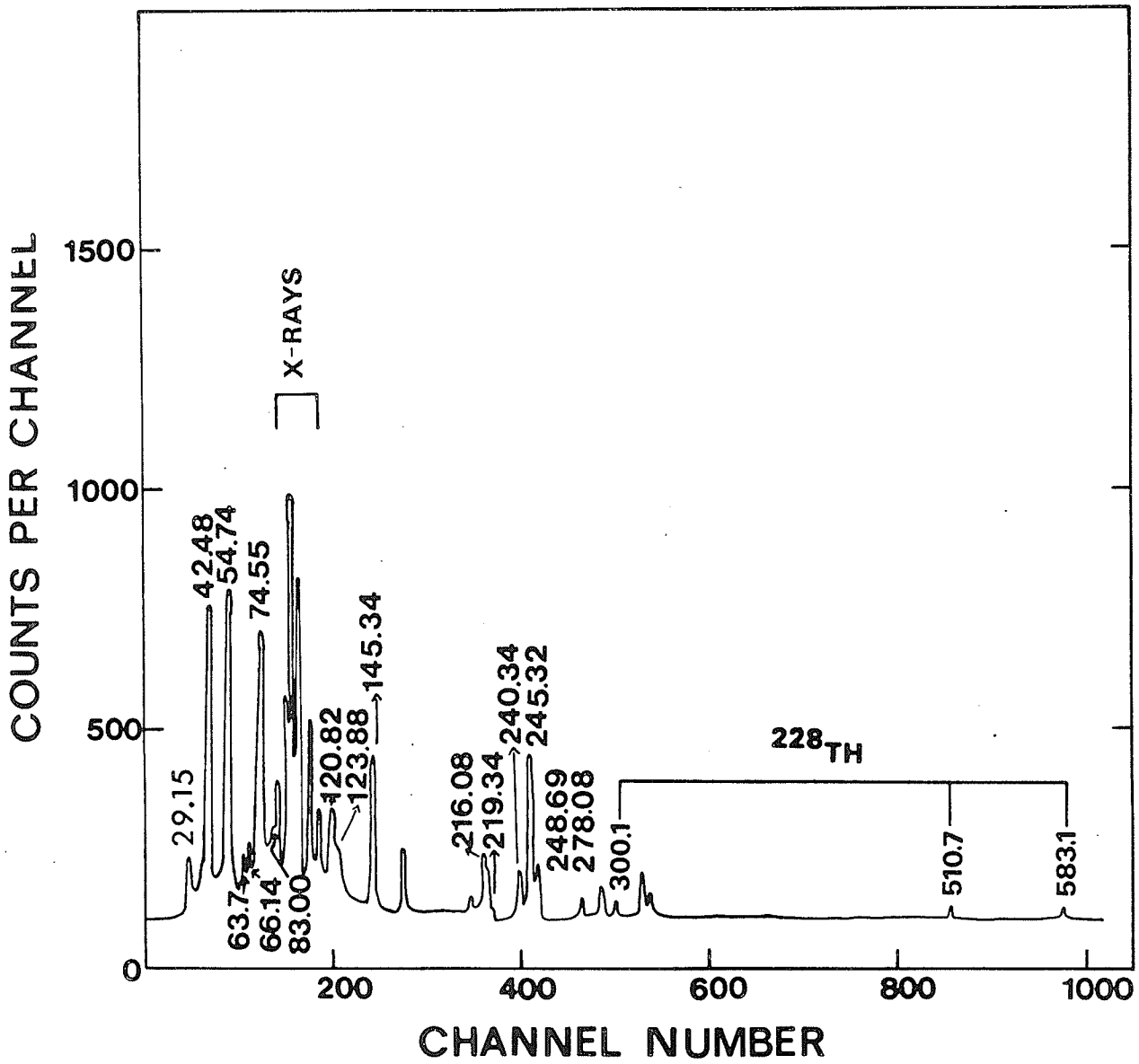
COUNTS PER CHANNEL
1500
1000
500
0
200
400
600
800
1000
CHANNEL NUMBER
X-RAYS
29.15
42.48
54.74
74.55
63.7
66.14
83.00
120.82
123.88
145.34
216.08
219.34
240.34
245.32
248.69
278.08
300.1
228TH
510.7
583.1

of the shielding and from the decay of Pb isotopes which were daughter products. The energies of the lines resulting from Th-228 are labelled in this figure, but in future diagrams they will be indicated merely as Th-228. Other photopeaks in the spectra which are not identified are randoms.

135.37 keV Gate:

The coincidence spectrum for the 135.37 keV gate is shown in Figure 14. The lines which are enhanced are the 29.15, 52.62, 72.88, 153.05, 156.14 and the 184.21 keV gammas. In order to accommodate the 184.21 keV gamma ray which is from the 425.85 keV level to the 241.52 keV level a linking transition of 76.98 keV is required from the 241.52 keV level to the 164.54 keV level. The 52.62 keV gamma had not been observed in the singles before, but it can be placed appropriately in the level scheme. The other gamma rays are also suitably placed in the level scheme.

139.79 keV Gate:

The coincidence spectrum for the 139.79 keV gate is shown in Figure 15. The lines in coincidence with the gating line have energies 29.15+29.36 doublet, 42.48+42.69 doublet, 71.84, 76.38, 118.98, 148.20, 153.05, 156.14, 176.13 and 177.81 keV. The 71.84 keV gamma ray is seen in the coincidence spectrum, but as mentioned earlier the 71.84 keV level has two possible ways to de-excite in addition to the ground state transition. It could emit a 29.36 keV gamma in cascade with a 42.48 keV gamma or it could emit a 42.69 keV gamma followed by a 29.15 keV gamma. Hence it is believed

FIGURE 14

COINCIDENCE SPECTRUM WITH THE 135.37 keV LINE

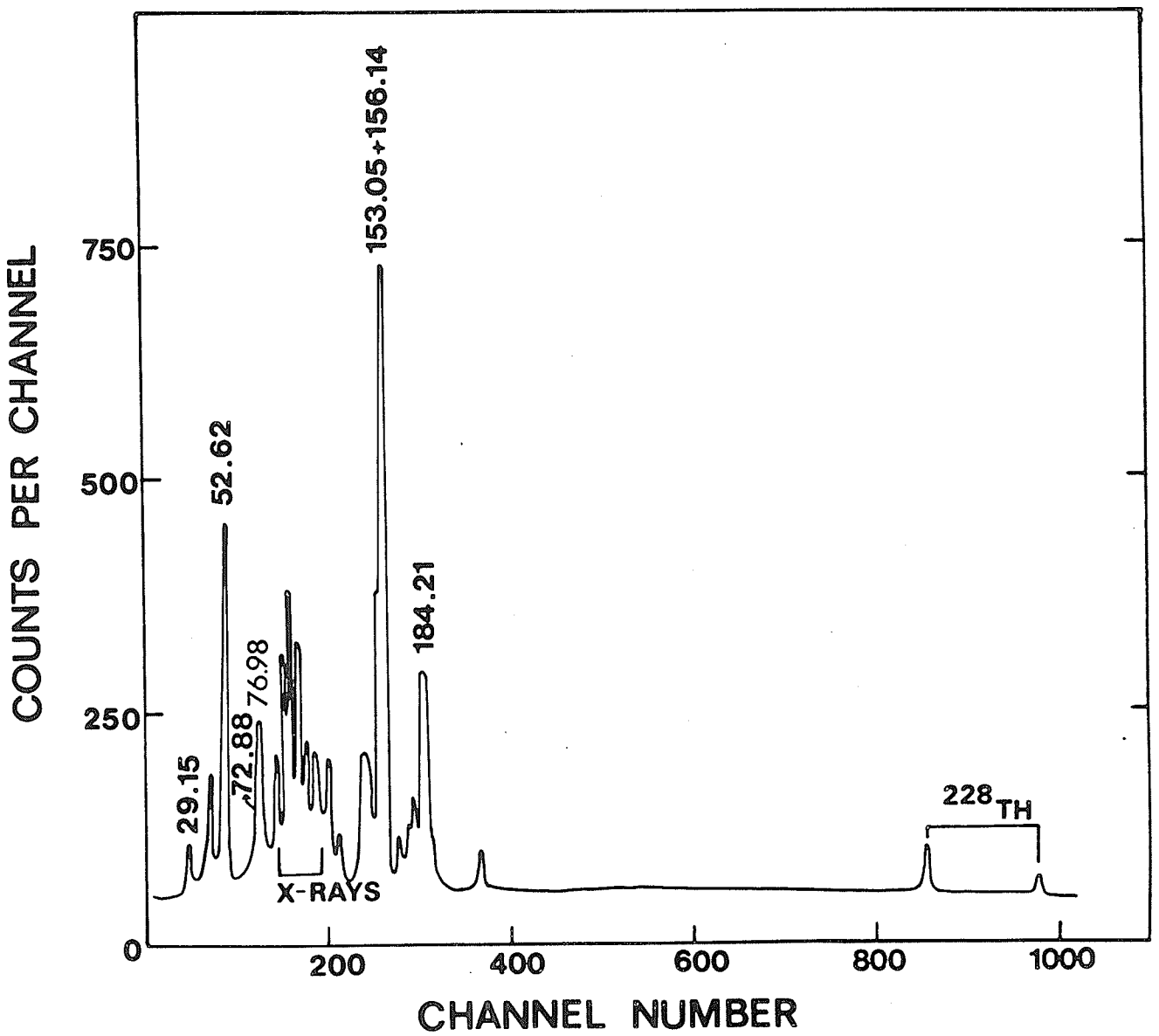
COUNTS PER CHANNEL
750
500
250
0
200
400
600
800
1000
CHANNEL NUMBER
29.15
52.62
72.88
76.98
X-RAYS
153.05+156.14
184.21
228TH

FIGURE 15

COINCIDENCE SPECTRUM WITH THE 139.79 keV LINE

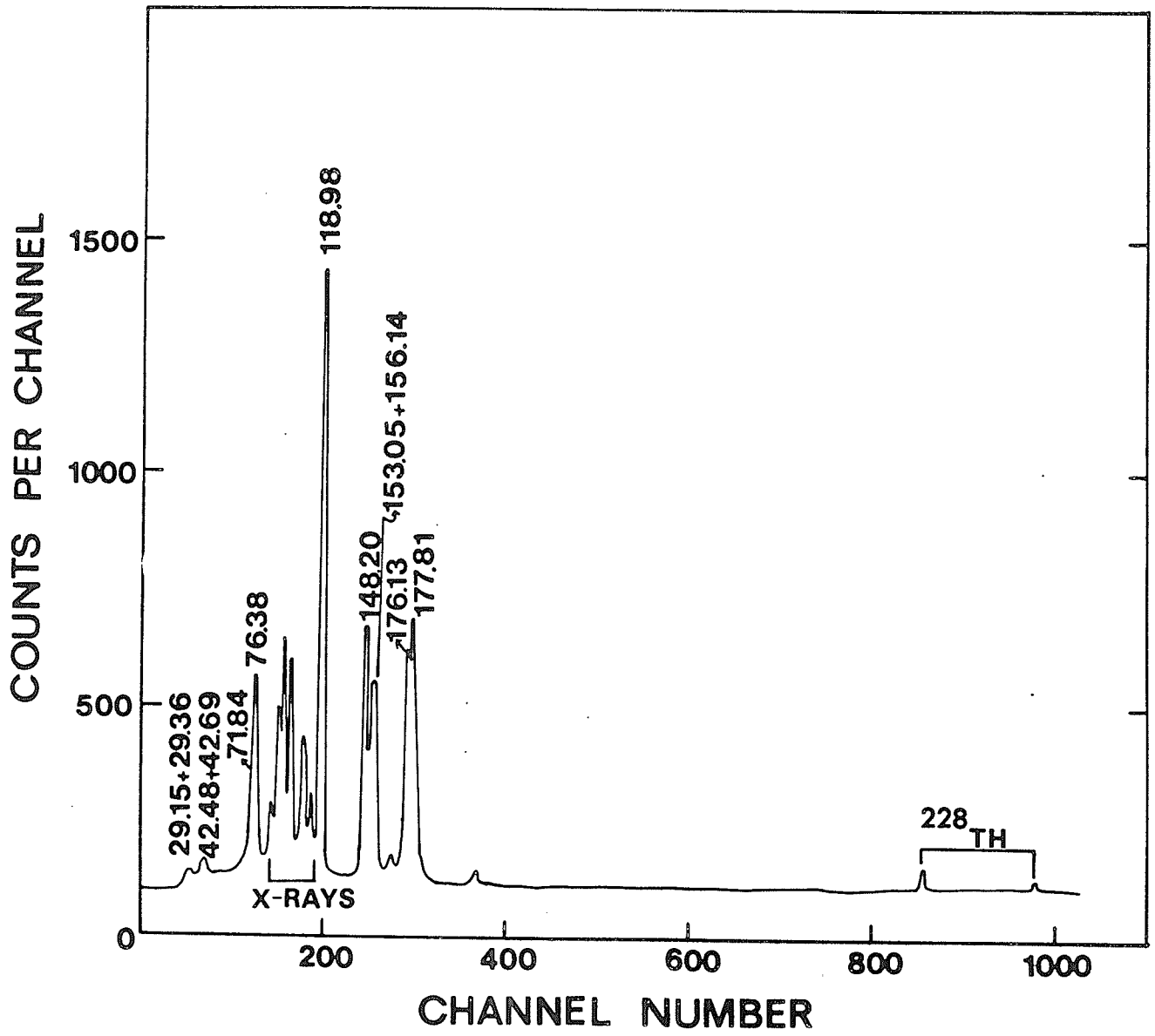
COUNTS PER CHANNEL
1500
1000
500
0
200
400
600
800
1000
CHANNEL NUMBER
29.15+29.36
42.48+42.69
71.84
76.38
118.98
148.20
153.05+156.14
176.13
177.81
X-RAYS
228 TH

that the lines at 29 keV and 42 keV are actually doublets which are not resolved.

The presence of the 153.05 and 156.14 keV gamma rays in the coincidence spectrum is explainable if it is assumed that a portion of the 135.37 keV line was also included in the gate. The 176.13 keV and 177.81 keV gamma rays are explained by postulating the existence of a second 139 keV gamma ray from the 478.74 keV level to a new level which is proposed at 340 keV which then de-excites giving the 176.13 keV and 177.81 keV gammas. The presence of the level at 340 keV cannot be considered proven but no other explanation of the presence of the 176 and 177 keV transitions seems reasonable.

(144.32+145.35+146.39+148.20) keV Gate:

The coincidence spectrum for this gate is shown in Figure 16. The gamma rays which are in coincidence with the gate are the 29.36+29.15 doublet, 42.48+42.69 doublet, 68.87, 71.84, 91.03, 139.79, 154.69, 169.05, 170.84, 172.30, 174.21, 192.13 and 219.36 keV lines. The presence of the 192.13 keV gamma ray indicates the existence of a gamma ray of 27.33 keV which de-excites the 173.78 keV level down to the 146.45 keV level. Although this 27 keV transition is not observed it is probably very heavily converted.

(162.27+164.54+165.72) keV Gate:

The coincidence spectrum for this gate is shown in Figure 17. The gamma rays in coincidence with the gate are the 29.36+29.15 doublet, 42.48+42.69 doublet, 52.62, 71.84,

FIGURE 16

COINCIDENCE SPECTRUM WITH THE (144.32+145.35+146.39+148.20)

keV LINES

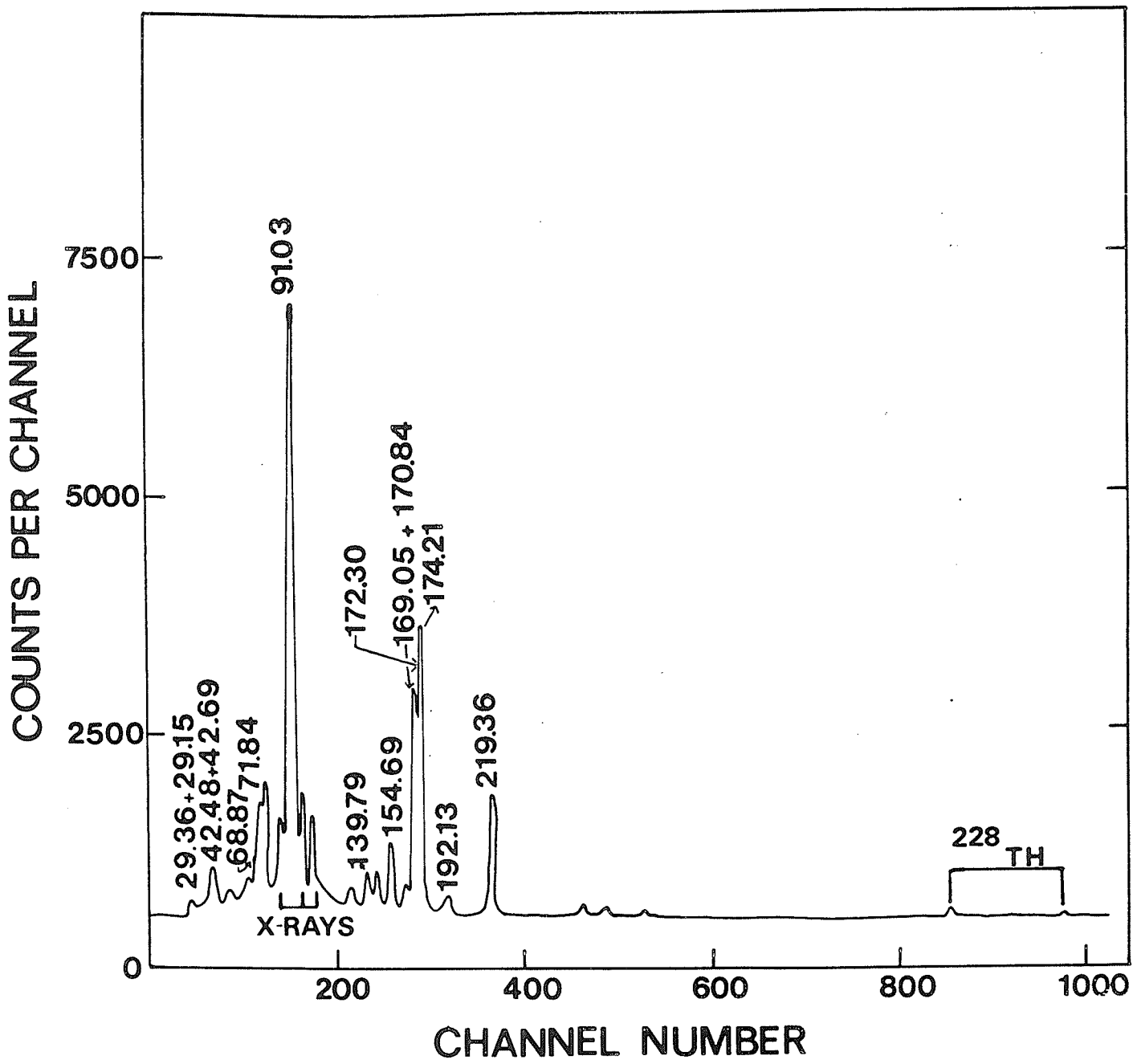
COUNTS PER CHANNEL
7500
5000
2500
0
200
400
600
800
1000
CHANNEL NUMBER
91.03
172.30
169.05 + 170.84
174.21
29.36+29.15
42.48+42.69
68.87
71.84
139.79
154.69
192.13
219.36
X-RAYS
228 TH

FIGURE 17

COINCIDENCE SPECTRUM WITH THE (162.27+164.54+165.72)

keV LINES

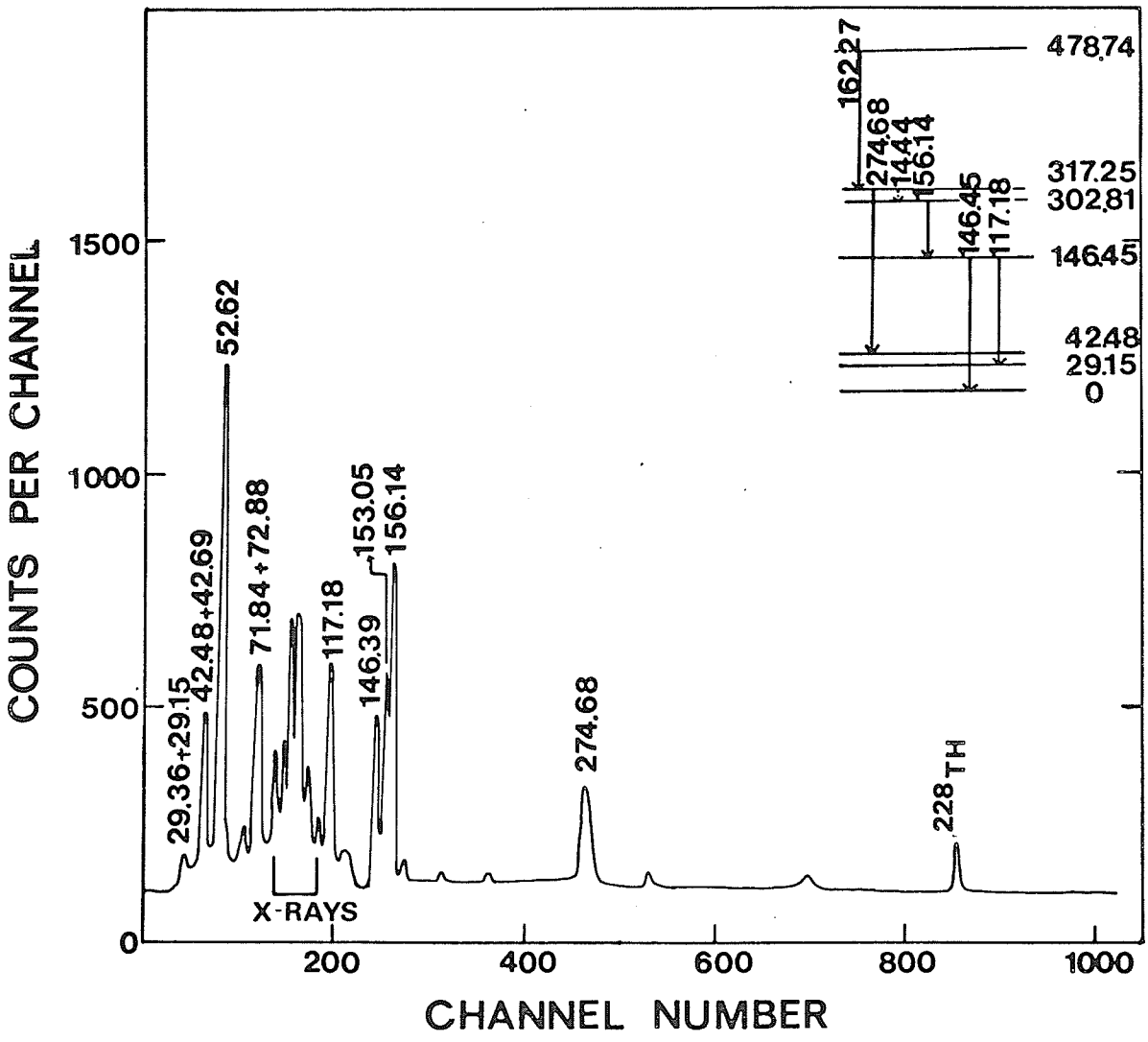
COUNTS PER CHANNEL
CHANNEL NUMBER
0
500
1000
1500
200
400
600
800
1000
29.36+29.15
42.48+42.69
52.62
71.84+72.88
117.18
146.39
153.05
156.14
274.68
228TH
X-RAYS
478.74
317.25
302.81
146.45
42.48
29.15
0
162.27
274.68
144.4
156.14
146.45
117.18

72.88, 117.18, 146.39, 153.05, 156.14 and 274.68 keV lines. In order to explain the presence of the 117.18, 146.39 and 274.68 keV lines it is postulated that this gate also includes the 162.27 keV gamma which results from the de-excitation of the 478.74 keV level to the 317.25 keV level.

The presence of the 117 and 146 keV gamma rays in the coincidence spectrum would be explained by the further cascade, 14.44 and 156.14 keV down to the 146.45 keV level from which the 117 and 146 originate. The 274.68 keV transition is that from the 317.25 keV level and this pattern of de-excitation is shown in the insert in Figure 17.

208.17 keV Gate:

The coincidence spectrum for the 208.17 keV gate is shown in Figure 18. The gammas in the coincidence spectrum are the 29.15, 50.42, 65.33, 77.13 and 128.3 keV gamma rays. The 50.42, 65.33, 77.13, 128.3 keV gamma rays were previously unobserved in the singles spectra, but were placed appropriately in the level scheme.

(216.08+217.13+219.34) keV Gate:

The coincidence spectrum for this gate is shown in Figure 19. The 217.13 keV transition is a ground state transition without coincident gamma rays so the gamma rays in coincidence with the 216.08 keV and 219.34 keV lines are the 29.36+29.15 keV doublet, 42.48+42.69 keV doublet, 71.84 keV, 74.55 keV, 117.18 keV and 146.39 keV gammas.

245.32 keV Gate:

The coincidence spectrum for this gate is shown in

FIGURE 18

COINCIDENCE SPECTRUM WITH THE 208.17 keV LINE

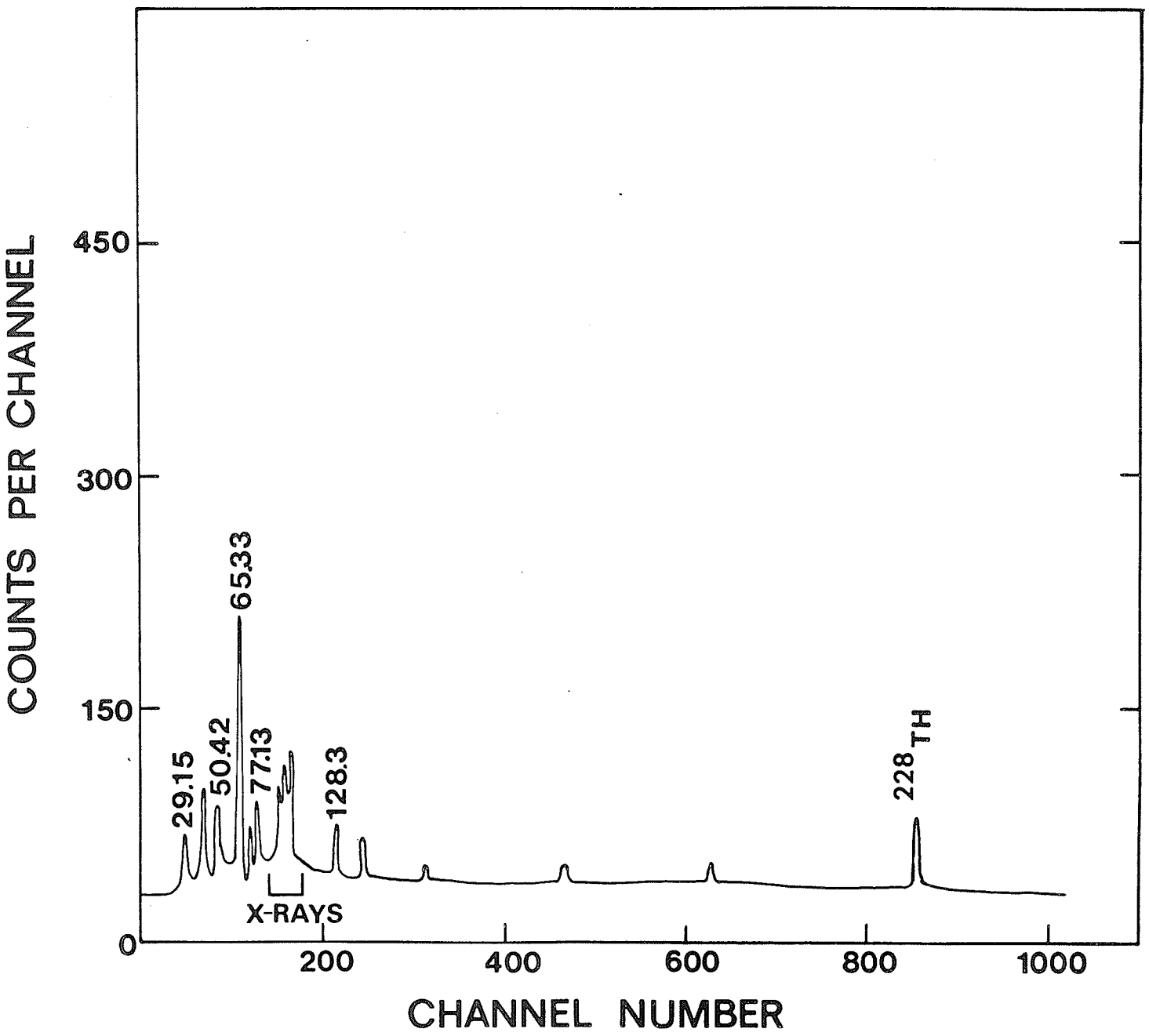
COUNTS PER CHANNEL
450
300
150
0
29.15
50.42
65.33
77.13
128.3
X-RAYS
228 TH
200
400
600
800
1000
CHANNEL NUMBER

FIGURE 19

COINCIDENCE SPECTRUM WITH THE (216.08+217.13+219.34)

keV LINES

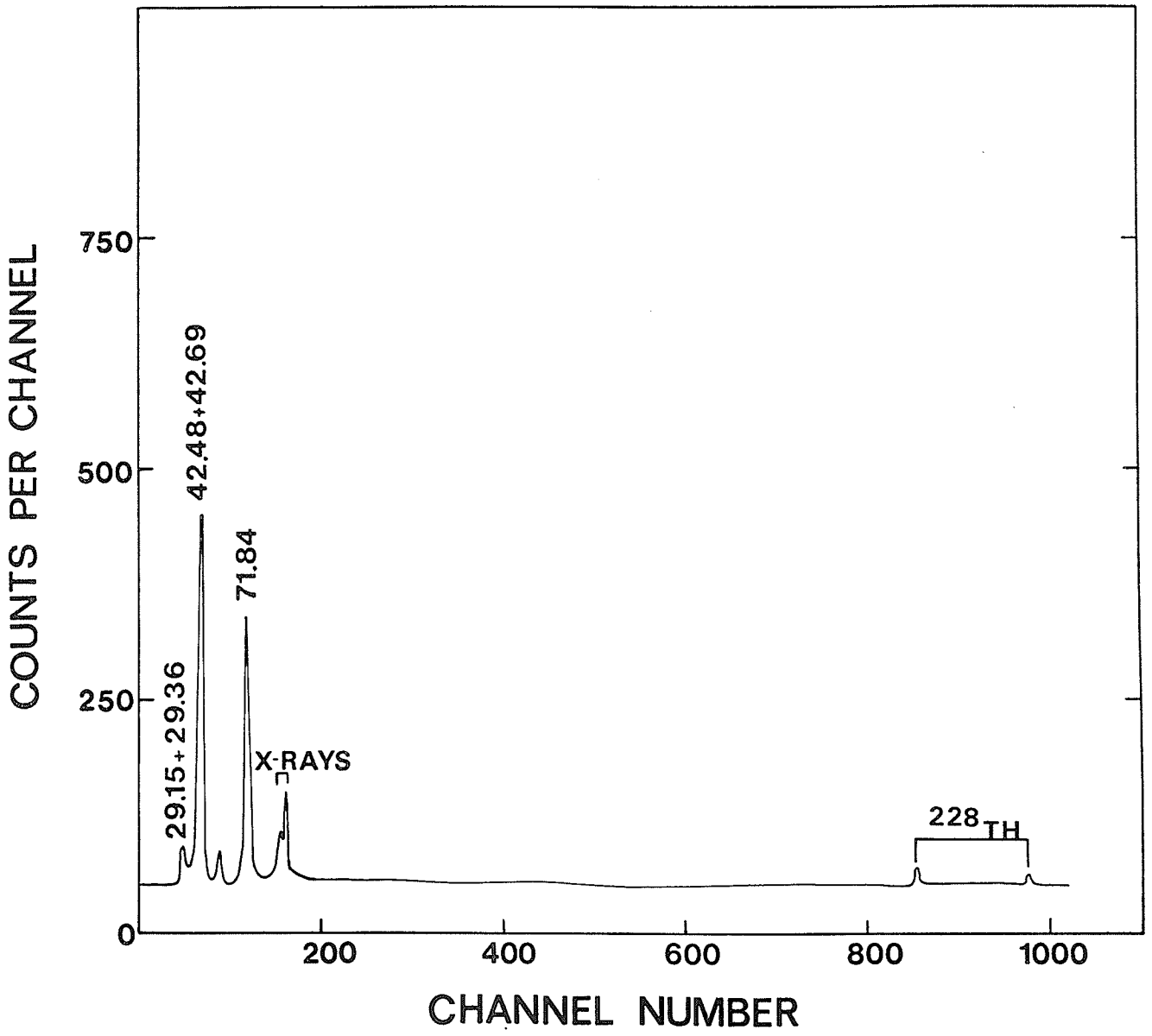
COUNTS PER CHANNEL
750
500
250
0
200
400
600
800
1000
CHANNEL NUMBER
29.15+29.36
42.48+42.69
71.84
X-RAYS
228TH

FIGURE 20

COINCIDENCE SPECTRUM WITH THE 245.32 keV LINE

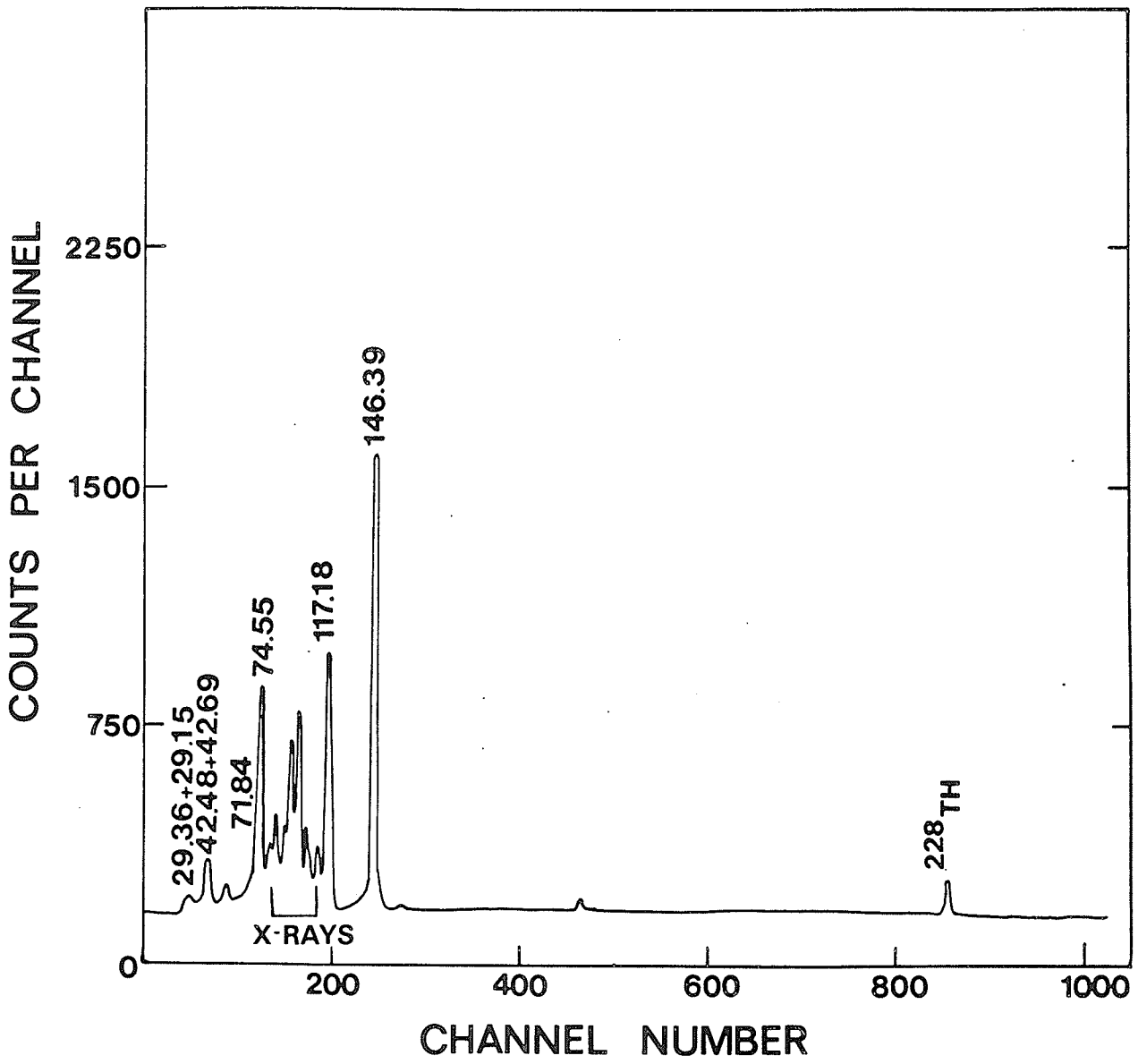
COUNTS PER CHANNEL
2250
1500
750
0
200
400
600
800
1000
CHANNEL NUMBER
29.36+29.15
42.48+42.69
71.84
74.55
117.18
146.39
X-RAYS
228TH

Figure 20. The 71.84 keV gamma is enhanced in the coincidence spectrum along with the 29 keV doublet and the 42 keV doublet as is to be expected from the level scheme.

278.08 keV Gate:

The coincidence spectrum is not shown for this gate. The only uranium gamma ray that is not random is the 42.48 keV gamma and this is to be expected from the level scheme.

291.34 keV Gate:

Similarly, this spectrum is not shown. The 29.15 keV gamma is the only genuine gamma ray in coincidence with the gate.

The results of the coincidence measurements are summarized in Table VIII, the coincidence table.

TABLE VIII

COINCIDENCE TABLE

GATE	GAMMA RAYS IN COINCIDENCE
42.48 keV	29.15, 54.74, 63.7, 66.13, 74.55, 83.00, 120.82, 123.88, 145.34, 216.08, 219.34, 240.43, 245.32, 248.69, 278.08 keV
135.37 keV	29.15, 52.62, 72.88, 153.05, 156.14, 184.21 keV
139.79 keV	29.15 + 29.36, 42.48+42.69, 71.84; 76.38, 118.98, 148.20, 153.05, 156.14, 176.13, 177.81 keV
(144.32+145.35+ 146.39+148.20) keV	29.15+29.36, 42.48+42.69, 68.87, 71.84, 91.03, 139.79, 154.69, 169.05, 170.84, 172.30, 174.21, 192.13, 219.36 keV
(162.27+164.54+ 165.72) keV	29.15+29.36, 42.48+42.69, 52.62, 71.84, 72.88, 117.18, 146.39, 153.05, 156.14, 274.68 keV
208.17 keV	29.15, 50.42, 65.33, 77.13, 128.3 keV
(216.08+217.13+ 219.34) keV	29.15+29.36, 42.48+42.69, 71.84, 74.55, 117.18, 146.39 keV
245.32 keV	29.15+29.36, 42.48+42.69, 71.84 keV
278.08 keV	42.48 keV
291.34 keV	29.15 keV

FIGURE 21

Th-229 LEVEL SCHEME

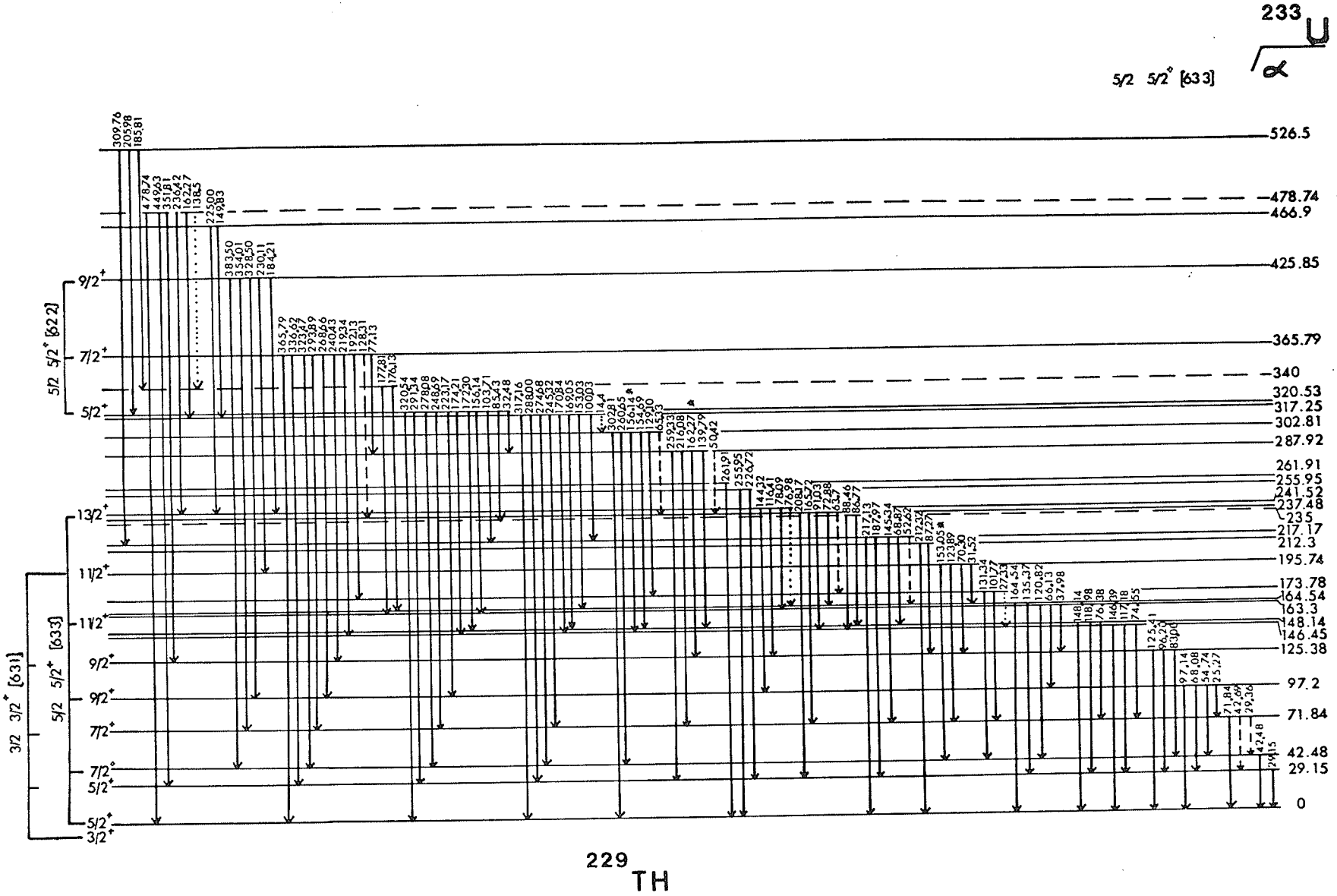
233 U
α
5/2 5/2+ [633]
526.5
478.74
466.9
425.85
365.79
340
320.53
317.25
302.81
287.92
261.91
255.95
241.52
237.48
235
217.17
212.3
195.74
173.78
164.54
163.3
148.14
146.45
125.38
97.2
71.84
42.48
29.15
0
5/2 5/2+ [622]
9/2+
7/2+
5/2+
3/2 3/2+ [631]
5/2 5/2+ [633]
13/2+
11/2+
11/2+
9/2+
9/2+
7/2+
7/2+
5/2+
5/2+
3/2+
229 TH

II. Th-229 Level Scheme

Using all the information available, viz., that obtained from the present work, the known energies of the alpha groups and the previous thesis results of Kroger (unpublished), the level scheme given in Figure 21 has been constructed. The gamma rays are labelled with their energies in keV. The gamma rays which were observed only in coincidence data are indicated by dashed lines. These gammas were probably unobservable in the singles spectra because of their high conversion coefficients and low intrinsic intensity. New gamma rays which have been proposed as linking transitions are indicated by dotted lines. Similarly, well established energy levels are drawn in solid lines while new levels which have been proposed are dashed. The proposed spin and parity of each level is shown at the left of the diagram and the energy at the right. The spins and parities are those inferred from the electron conversion data of Ahmad (unpublished) and quoted by Kroger.

III. Discussion of Rotational Nuclei and the Th-229 Level Scheme

U-233 is an odd A deformed nucleus which has a permanent deformation in the ground state. In the development of the theory of odd A nuclei, the assumption of strong coupling is made. Using this assumption, the motion of the odd nucleon as viewed from a reference frame fixed in the nucleus and rotating with it is identical with that of a single nucleon moving in a similar but non-rotating potential.

The total Hamiltonian for this problem involves a term dealing with the nucleus as a whole, one term involving the nucleons and also an interference term. The collective modes and the oscillations of the individual nucleons are related because if the nucleus is distorted from sphericity, the particles are no longer in the same average potential and the motions of the nucleons will be altered. The "shape of the nucleus" is nothing but the density distribution of the particles so there is definitely an interaction between collective and particle degrees of freedom. If the interference term is neglected, the energy eigenvalues of the Hamiltonian are:

$$E_{I,I_0} = \frac{\hbar^2}{2\mathcal{I}_0}\,[I(I+1)-2K^2]+E_{I_0}$$

where I is angular momentum, K is the projection of I on the symmetry axis and $\mathcal{I}_0$ is the moment of inertia. For each non zero value of K all values of $I \geq K$ are allowed. Thus built on each single particle state in the deformed potential is a

rotational band of energy levels. Within a band, the spacing of the levels is given by

$$E = \frac{\hbar^2}{2\mathcal{I}_o} [I(I+1) - I_o(I_o+1)]$$

The energy difference E measures all energies relative to the band head energy and I_o is the base spin of the band.

The ground state of U-233 has been well established to be a spin $\frac{5}{2}$ state and hence is the Nilsson orbital $\frac{5}{2}\frac{5}{2}^+[633]$. Since 83% of the alpha decay from U-233 to Th-229 goes directly to the ground state, this is the preferred alpha transition. Hence the ground state of Th-229 will have the same spin I and K and Alaga values as the ground state of U-233 so the Nilsson assignments of the ground states of Th-229 and U-233 are both $\frac{5}{2}\frac{5}{2}^+$ [633].

The ground state rotational band $I_o=\frac{5}{2}$ is a very good example of a rotational band where the neglecting of the interference term is justified. For $I_o=\frac{5}{2}$, I can take on any value greater than $\frac{5}{2}$. For $I=\frac{7}{2}$, E=42.48 keV so $\frac{\hbar^2}{2\mathcal{I}_o}$=6.07. For $I=\frac{9}{2}$ E=97.2 keV so $\frac{\hbar^2}{2\mathcal{I}_o}$ = 6.08. For $I=\frac{11}{2}$ E=163.3 keV so $\frac{\hbar^2}{2\mathcal{I}_o}$=6.05 and for $I=\frac{13}{2}$, E=241.52 keV so $\frac{\hbar^2}{2\mathcal{I}_o}$ = 6.04. The average value of the rotational constant $\frac{\hbar^2}{2\mathcal{I}_o}$ is 6.06±0.02. Since the values of the constant agree so well, we see that we were justified in assuming that the interference term which is also known as the coriolis coupling term could be neglected and that the energies we have assigned to the various levels are reasonably accurate. Continuing the calculation up to the next possible I value of $\frac{15}{2}$ we would expect another energy

level at 333.14 keV but it does not appear to be populated to any measurable extent.

From the level scheme one would expect the next rotational band to be the following levels; $\frac{5}{2}$+(29.15 keV), $\frac{7}{2}$+(71.84 keV), $\frac{9}{2}$+(125.38 keV) and $\frac{11}{2}$+(195.74 keV) and this was first suggested by Ahmad according to Kroger. An examination of the Nilsson diagram, however, reveals the total absence of $\frac{5}{2}$+ states in the vicinity of the ground state $\frac{5}{2}$ $\frac{5}{2}$+[633]. At considerably higher energies in the diagram we find the $\frac{5}{2}$ $\frac{5}{2}$+[622] state (and this is to be located at about 300 keV above the ground state in the level diagram according to Baranov et al[20]) so this is unlikely to represent an intrinsic level at about 29 keV above the ground state. Further, the calculated values of the rotational constant for these levels ($\frac{\hbar^2}{2\mathcal{I}_o}$), assuming a $\frac{5}{2}^+$ band come to 6.10, 6.01 and 6.17 keV. This is somewhat erratic but not sufficiently so to completely rule out the levels as members of a rotational band. Kroger presents arguments which indicate that the proper interpretation is that these are the $\frac{5}{2}$,$\frac{7}{2}$,$\frac{9}{2}$ and $\frac{11}{2}^+$ spin states of a $\frac{3}{2}^+$ rotational band, the intrinsic level of which is close to the ground state. It indeed would appear that this interpretation, at first sight somewhat fanciful, is in fact correct. As Kroger has pointed out the 71.84 keV gamma ray is relatively strong and appears from electron conversion work to be pure E2. This is not to be expected if the transition is from a $\frac{7}{2}^+$ level to a $\frac{5}{2}^+$ level, but it is explained if in reality it goes to a $\frac{3}{2}^+$ level,

which in the present data would lie not more than 40 eV above the $\frac{5^+}{2}$ ground state. Kroger quotes unpublished data received by private communication (J.R. Erskine) that in the ^{230}Th(d,t)^{229}Th reaction the apparent levels populated are the $\frac{5}{2}$, $\frac{7}{2}$ and $\frac{9^+}{2}$ band members of this $\frac{3^+}{2}$ band and to one or two keV in energy the band head would coincide with the ground state. If this evidence is supported, the correctness of the present postulate is quite likely. The Nilsson diagram gives the $\frac{3}{2}$ $\frac{3}{2}$ + [631] state immediately adjacent to the $\frac{5}{2}$ $\frac{5}{2}$ + [633] state so this description is assigned to this band.

Finally, the $\frac{5}{2}$, $\frac{7}{2}$, and $\frac{9^+}{2}$ levels at 320.53, 365.79 and 425.85 keV appear to belong to the $\frac{5}{2}$ $\frac{5}{2}$ + [622] band mentioned earlier. The calculated values of the rotational constant is 6.47 and 6.58 for the two energy intervals. The $\frac{11^+}{2}$ level is therefore expected at about 500 keV, but there is little positive evidence to identify it.

It will be noted that new levels are proposed at 235, 340 and 478.74 keV. The evidence for each is supported by several gamma rays as will be seen from the level scheme. In addition, the present work strengthens that of Kroger. For example, the 526.5 keV level is now much more firmly established and the energies of all the levels have been revised and now have excellent consistency with the gamma ray pattern. New gamma rays have been placed in the scheme and insofar as the level scheme has been developed a greater degree of completeness prevails. While the present work is at variance with that of

Kroger in not a few respects there can be no doubt as to the basic soundness of most of his suggestions and conclusions. In particular, the present work has confirmed the level scheme with the amendments noted with a finer degree of certainty.

In so complex a disintegration scheme it would be rash to believe that the last word has been said. Certainly there still remain uncertainties in the decay of U-233 with a few gamma rays still to be placed and therefore a few levels still unrecognized. The present work is offered as a stepping stone on the road to the complete understanding of this, one of the most complicated decays in the heavy elements.

References

1. W. Teoh, Ph. D. Thesis, University of Manitoba, 1973.
2. S. G. Thompson, K. Street, Jr., A. Ghiorso and G. T. Seaborg, Physical Review, 80, 79 (1950).
3. G. T. Seaborg, J. W. Gofman and R. W. Stoughton, Physical Review, 71, 378 (1947).
4. E. K. Hyde, NNES 14B, 1431 (1949), quoted in Nuclear Data Sheets Reference List for A=233.
5. E. K. Hyde, I. Perlman and G. T. Seaborg, "The Nuclear Properties of the Heavy Elements Volume II ", Prentice Hall Inc. N. J. (1964).
6. I. Ahmad, Ph. D. Thesis, Report UCRL-16888 (1966).
7. J. E. Cline, Idaho Nuclear Corp. Report IN-1448 Rev. (1971).
8. L. A. Kroger, Ph. D. Thesis, University of Wyoming, 1972.
9. C. E. Crouthamel, "Applied Gamma-Ray Spectrometry", Pergamon Press (1970).
10. W. Teoh, Nuclear Instruments and Methods, 109, 509 (1973).
11. R. C. Greenwood, R. G. Helmer and R. J. Gehrke, Nuclear Instruments and Methods, 77, 141 (1970).
12. International Atomic Energy Agency (1969).
13. J. A. Bearden, Reviews of Modern Physics, 39, 78 (1967).
14. K. Siegbahn, "Beta and Gamma Ray Spectroscopy", North Hollander Inc., N. Y. (1955).
15. Nuclear Data Sheets for A=133 (1974).
16. J. L. Campbell and L. A. McNelles, Nuclear Instruments and Methods, 117, 519 (1974).

17. G. T. Chapman, Nuclear Instruments and Methods, 52, 101 (1967).

18. G. W. Grodstein, National Bureau of Standards Circular 583 (1957).

19. K. A. Kraus and F. Nelson, Proceedings of the International Conference on Peaceful Uses of Atomic Energy, Geneva, 1955, 7, 113 (1956).

20. S. A. Baranov, M. K. Gadzhiev, V. M. Kulakov and V. M. Shatinskiĭ, Soviet Journal of Nuclear Physics, 5, 365 (1967).